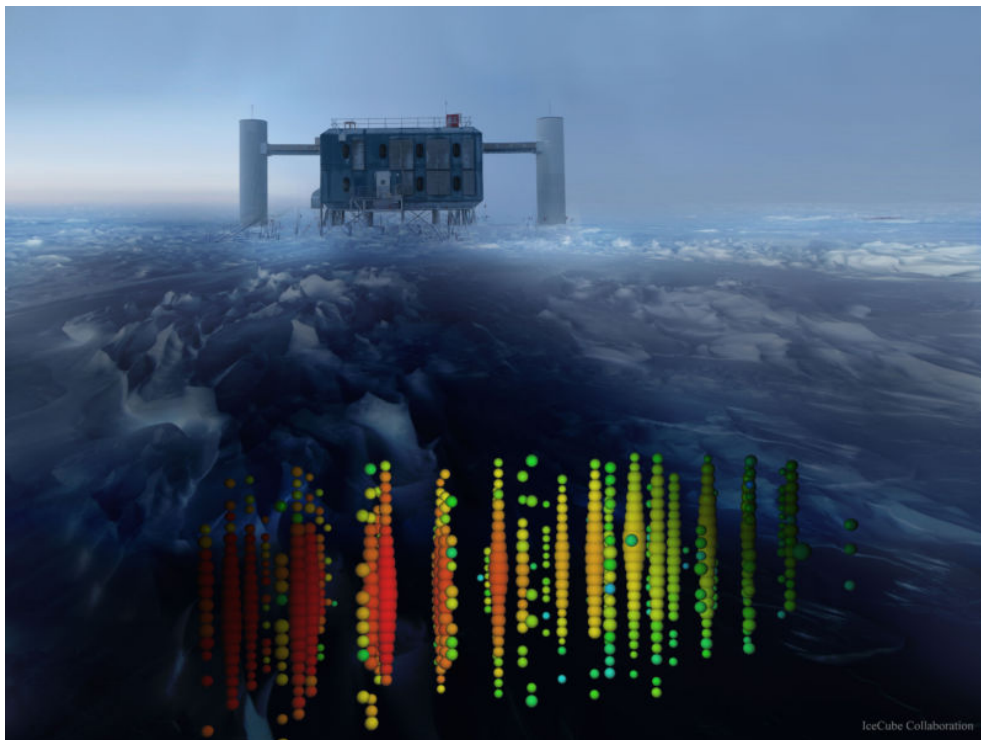




Searches for Lorentz
Invariance Violation of Gamma
Ray Burst neutrinos with the
IceCube neutrino detector



THESIS
submitted in partial fulfillment of the
requirements for the degree of
MASTER OF SCIENCE
in
PHYSICS

Author :	Thijs Poiesz
Student ID :	1755153
Supervisor :	Dr. D.F.E. Samtleben R. Gracia Ruiz
2 nd corrector :	Prof. Dr. A. Achúcarro

Leiden, The Netherlands, July 17, 2020

Searches for Lorentz Invariance Violation of Gamma Ray Burst neutrinos with the IceCube neutrino detector

Thijs Poiesz

Instituut-Lorentz, Leiden University
P.O. Box 9500, 2300 RA Leiden, The Netherlands

July 17, 2020

Abstract

We look for cosmic neutrinos originating in Gamma Ray bursts using public data from the IceCube collaboration. We allow for a time difference between a neutrino and GRB photon of up to 40 days to probe possible Lorentz invariance violations. These violations might become visible if a neutrino has high enough energy and traveled a long enough distance before we observe it. We make use of pseudo experiments to simulate different possible neutrino realizations and see how well a signal can be discerned from background. We find slightly less neutrinos than expected from background in the IceCube data. A signal associated with more than 3% of the GRBs can be excluded at 98% confidence in the northern hemisphere, and at 70% confidence in the southern hemisphere.

Under the assumption that the highest energy neutrinos that can be associated to a GRB are experiencing LIV induced time shifts we have derived an intrinsic time difference at emission between GRB neutrinos and photons of $\Delta t_{in} = (4.49 \pm 23.0) 10^4 s$, and a LIV scale of $E_{LIV} = (1.05 \pm 0.85) 10^{15} GeV$, while the probability of finding similar results from purely uncorrelated events is $P = 54\%$.

Contents

1	Introduction	3
2	Physics	7
2.1	Lorentz Invariance Violation	7
2.2	Neutrinos	9
2.3	Gamma Ray Bursts	10
3	Observations	13
3.1	IceCube	13
3.1.1	IceCube neutrinos	15
3.2	Gamma Ray Burst observations	17
3.2.1	Gamma Ray Bursts for IC40	19
4	Method	23
4.1	Statistical approach	25
4.1.1	Goodness of fit test	25
4.1.2	The test statistic	27
4.2	Matching criteria	29
4.2.1	Search cone size	29
4.2.2	Time window	30
4.3	Pseudo experiments	32
4.3.1	Simulating background	32
4.3.2	Simulating signal	34
4.4	Performance	35
4.4.1	Expectations from background	35
4.4.2	Sensitivity	38
4.4.3	Results from IceCube 40	40

5	IC79 and IC86	47
5.1	Effective area	48
5.2	Energy selection	50
5.3	Sensitivity for IC79 and IC86	54
5.4	Results	62
6	Conclusion	67
6.1	Discussion	69
A	Deriving the test statistic	71
B	Least-squares fitting	73
B.1	Correlation coefficient	74
C	Constant search cone on IC79/86	77
C.1	Results for constant search cone	85

Introduction

To better understand the universe a mathematical formulation of all elementary particles and the way they interact is useful. In 1975 Abraham Pais and Sam Treiman first coined the term standard model for the model describing these fundamental interactions [1]. The standard model is a Lorentz invariant formulation of three of the four fundamental physical forces [37]. It describes the electromagnetic, weak and strong interactions and has done many experimentally confirmed predictions such as the existence of top quarks [2, 3], neutrinos [4], and the Higgs boson [5].

The standard model is not a complete description of the whole universe however. It fails to explain baryon asymmetry [6], or the accelerated expansion of the universe [7, 8]. It also lacks a description of gravitational forces as in general relativity. The two different theories work well within their own regimes. For a particle of mass M , quantum effects, as described by the standard model, are relevant at the scale of the Compton wavelength $\lambda_c = \frac{\hbar}{Mc}$. Here \hbar is Planck's constant and c is the speed of light. Gravitational effects will become relevant on scales of the Schwarzschild radius, $r_s = \frac{GM}{c^2}$. If a spherically symmetric, non rotating, object of mass M becomes smaller than this radius, it will form a black hole. For most known objects these two scales differ to a great extent and only one of the two theories has to be used. If we want a complete description of nature however it is interesting to look at the scales for which both theories are relevant. By simply setting the Compton wavelength equal to the Schwarzschild radius we will find the Planck mass, $M_p = \sqrt{\frac{\hbar c}{G}} \sim 10^{28} eV$. This mass is associated with the Planck scale. This is a scale given in Planck length, $l_p = \sqrt{\frac{\hbar G}{c^3}}$, time, $t_p = \sqrt{\frac{\hbar G}{c^5}}$, temperature, and charge, that tells us when general relativity and quantum field theory (QFT) give con-

flicting results.

Models unifying quantum field theory and general relativity are called quantum gravity theories. Multiple attempts have been made to develop testable quantum gravity theories [9]. Using the standard scheme of quantization on gravity was the most tried approach up to the early 1970s when it was shown that this scheme will lead to some inconsistencies in the theory [10, 11]. Other attempts such as (super)string theory or loop quantum gravity are more promising, but lead to adjustment of QFT and relativity. One of the common approaches to quantum gravity is allowing for violation of Lorentz invariance (LIV). This is done by introducing a background field, as a series expansion, on an energy scale similar to the Planck scale [12–16]. The newly introduced field gives the system a preferred frame of reference and violates Lorentz invariance [17–19]. Following [15, 20, 21] we write the velocity dispersion relation in quantum gravity theories in equation 1.1. Here, the energy of a particle is denoted by E , m is the particles rest mass, the momentum is given by p , c is the speed of light. ϵ is an unknown constant which relates the Scale of LIV to the Planck scale, $\epsilon M_{pl} = E_{LIV}$.

$$E^2 - m^2 c^4 \approx -p^2 c^2 - E^2 \sum_{n=1}^{\infty} s_n \left(\frac{E}{\epsilon_n M_{pl}} \right) \quad (1.1)$$

Because both relativity and the standard model are Lorentz invariant theories that seem to work just fine within the appropriate regimes, it is worthwhile to investigate this violation more closely. We expect to see the LIV effects more clearly in the regimes where both theories are conflicting. This means we will be looking at ways to probe scales that come as close as possible to the Planck scale. It is at present not possible to do laboratory experiments accessing the Planck scale. We can however look at highly energetic cosmic events. If these events happen far away from Earth it might be possible to observe the effects of LIV. The large traveling distance means that redshift effects will enhance even a small deviation from relativity, as in equation 1.1.

It is interesting to investigate how well we know that massless particles are Lorentz invariant, and how well we know that massive particles in the high energy limit behave the same. To do these kind of investigations it is necessary to measure separate types of signal from the same source. Observing a source in multiple different ways is a relatively new field of astrophysics called multi-messenger astronomy. In this thesis photons are used as massless particles and cosmic neutrinos as massive particles. Neutrinos can have a wide range of energies depending on their source. The

highest neutrino energies are the least probed part because these energies can only be reached in cosmic accelerators. The first time neutrinos were associated directly with a cosmic source was in 1987 when multiple instruments detected neutrinos coinciding with supernova 1987A [22, 23]. The combined observation of a photon and a neutrino from the same source opened the door for investigating differences in their propagation through space.

What makes neutrinos extra fitting for investigating Lorentz Invariance is the fact that they are thought to have small mass which makes interaction through gravitational forces negligible [24], furthermore they only interact through the weak force. These properties make neutrinos travel long distances almost without interacting. Since they travel uninterrupted through space, neutrinos from far away regions are good messenger particles. Even when they originate in dense regions a big proportion of them will travel through this region without interacting. If a cosmic source is found to be emitting both neutrinos and photons simultaneously

The suggestions that they can be emitted simultaneous with photons from a Gamma Ray Burst (GRB) gives us a chance to look at differences between photon and neutrino propagation [25, 26]. GRBs are extremely energetic and of unknown origin, with a duration in the order of a few seconds, occurring well outside the milkyway. Already in 1997 Waxman [27] suggested that high energy (TeV to PeV) neutrinos can originate in GRBs. The high neutrino energy in combination with the great distance to the burst makes this scenario a good candidate for testing LIV effects. Even tiny LIV effects will become noticeable when the distance traveled is big enough.

Since the publication of these studies, there have been many more measured gamma ray bursts. Even more significant in this regard is the further completion of the IceCube detector. The increasing size of the detector has allowed for the detection of many more neutrino events. The increased number of observed neutrino events makes it possible to expand a previous assessment of LIV in GRB neutrinos done by [28]. This assessment used data collected by the Antares telescope[29] and IceCube in its 40 string configuration[30]. We will first follow the work done in [28] to set up our method of associating neutrinos to GRBs and then apply it to newer data. We use neutrino data collected by the IceCube detector in its 79 and 86 string configuration and GRB data obtained from the GRB-web [31] and GRB Coordinates Network (GCN) [32]. Both GRB catalogs contain data from a multitude of detectors.

A boundary on LIV of cosmic neutrinos from a Blazar has been derived in [33]. A high energy ($E \geq 200\text{TeV}$) neutrino detected by the IceCube de-

tector and photons from the coinciding blazar TXS 0506+056 are used to see how much the neutrinos propagation speed deviates from the speed of light. Using a linear relation between the neutrino energy and propagation speed, and allowing for a time difference in neutrino and photon propagation of 10 days an upper limit for the Lorentz Invariance violation of $E_{LV} \geq 3 \times 10^{16} GeV$ was found. More recent attempts have been made to exploit the correlation of GRB photons and neutrinos to constrain the LIV scale. In 2019 [34] for example, public IceCube data is used to find a LIV energy scale of $E_{LV} = (6.4 \pm 1.5) \times 10^{17} GeV$. One of the caveats of the method used there is that the LIV scale was derived using 12 shower neutrino events originating in the northern hemisphere. These type of events can be reconstructed with an angular resolution of around 10° , making the associating of a neutrino to a GRB less significant.

We will first describe the effect Lorentz invariance violation can have on observations in multimessenger astronomy in chapter 2. In the same chapter, we consider why photons and neutrinos are good candidate particles to explore the possible LIV effects. In chapter 3 we will look at the type of data that is collected by the IceCube detector and how it can be interpreted. An overview of the GRB data we have selected is also given in this chapter. In chapter 4 we describe a statistical approach for correlating neutrinos to GRBs. This approach follows one derived in [28]. We apply the statistical approach to the IC40 data for a comparison with previous results. In the last chapter we use the newer IceCube data, collected from June 2010 to May 2013 covering a broader range in the sky. We will first blind the data to tune our method to the new information and after that we look at the results of associating GRBs with neutrinos. At last we will derive the scale of LIV effects from our found results and discuss its significance.

Physics

We start this chapter by considering how LIV effects can become visible. An educated guess of the LIV scale was given in the introduction and set proportional to the Planck scale. This is derived by considering on what scales both theories are valid and relevant. As can be seen in equation 1.1 we introduced LIV effects as a correction to the velocity dispersion relation. This correction is given as a series expansion of the particles energy over the LIV scale. Since the LIV scale is expected to be very high we need highly energetic particles to probe LIV effects even up to first order. If we compare for example the arrival times of two particles with very different energies coming from the same source we might see a small deviation from the expectations from general relativity. Multi messenger astronomy gives us a way of comparing two particles of very different energies. We will look at the neutrino and GRB photons as candidate particles in the sections 2.2 and 2.3.

2.1 Lorentz Invariance Violation

The goal is to investigate the possibility of a shift in propagation time due to LIV effects. These effects will be investigated between neutrinos and GRB photons from the same source. How to identify GRBs that could have emitted a neutrino will be treated in section 4.2. For now we assume that GRBs emit high energy neutrinos. We had already described the velocity dispersion relation through a phenomenological approach in equation 1.1. For GRB photons the mass term in this equation is zero. For the high energy cosmic neutrinos we can safely neglect the mass term, since it is much smaller than the neutrino energy [35]. We also know that the particle

energies that have been measured until now are at least a few orders of magnitude smaller than the Planck scale. This makes dropping the higher order terms in the expansion in equation 1.1 a valid approximation [14, 34, 36]. Next, assuming $dE/dp = v(E)$ still holds in quantum gravity theories, we can derive the velocity of a high energy particle traveling towards us from a cosmic source.

$$v_n(E) \approx c \left[1 - s_n \frac{n+1}{2} \left(\frac{E}{E_{LIV,n}} \right)^n \right] \quad (2.1)$$

In equation 2.1, $v_n(E)$ is the particles n th order velocity term is given as a function of its energy, E . The sign of the LIV term is given by $s_n = \pm 1$. $E_{LIV,n}$ is the scale of of the n th order Lorentz correction, which has to be found from the data. Now that we have a relation for the particles traveling speed we can calculate the expected time shift due to LIV between the two particles. We consider only the first order part since this will have the biggest contribution to the traveling time difference. Equation 2.2 gives the time shift due to LIV effects. For two particles coming from the same source, with different energies, E_h , and E_l , we find.

$$t_{LIV} = \pm \frac{E_h - E_l}{E_{LIV}} \frac{D(z)}{c} \quad (2.2)$$

If we consider the case of GRB neutrinos and photons we can neglect the photon energy E_l , Since it is much smaller than the neutrinos energy, E_h [36]. Since the particles travel a long distance at different speed we have to account for the expansion of the universe. As a particle travels slower, its traveling time will be delayed by this expansion even more. We included this expansion by writing the distance, $D(z)$, to a far away source as a function of both the redshift of the source, z , and the content of the universe. The content of the universe is usually described in terms of cosmological parameters, Ω_i , where i denotes the type of content [8]. These parameters give the ratio of the density of a certain content species (ie. matter, photons, cosmological constant) divided by the critical density. Where critical density is the density at which the universe will halt expansion after an infinite time.

$$D(z) = \frac{c}{H_0} \int_0^z \frac{(1+z') dz'}{\sqrt{\Omega_m (1+z')^3 + \Omega_\Lambda}} \quad (2.3)$$

Here H_0 is the Hubble constant at present, Ω_m , and Ω_Λ are the matter and cosmological constant density parameters at present, and z is the redshift.

We will look at the appropriate events in some more detail in the next sections. We will discuss some background information on neutrinos, GRBs, and the observations of both events.

2.2 Neutrinos

Neutrinos are electrically neutral subatomic elementary particles, that were first predicted by Wolfgang Pauli in 1930. Neutrinos only interact through the weak subatomic force and gravity. They are thought to have very low mass [35] and since the range of the weak force is also small they are expected to travel almost unperturbed through space. Due to these properties they were only discovered in 1956 [4], while they were already well established in theoretical models. Neutrinos can be created in three different flavors. Each flavor is associated with nuclear reactions of leptons with the same flavor, so that the lepton flavor over the reaction is conserved. Electron neutrinos, muon neutrinos and tau neutrinos correspond to the electron, muon, and tau particle respectively. There also exist antineutrinos which have opposite lepton number and correspond to the opposite lepton particle. For example an electron, and positron corresponds to an electron neutrino and an electron antineutrino. The conservation of lepton flavor is only approximately conserved. The most notable violation of this conservation can be seen in neutrino oscillations. This describes the change of lepton flavor of a single neutrino traveling through space [24, 37].

There are many different sources of neutrinos. A classification of neutrino sources can be made based on the measured neutrino energy. In figure 2.1 an overview of the different energy neutrinos, and their fluxes is given. The appropriate source for each energy band is also given in this plot. It is important to note that not all sources have been experimentally confirmed yet. Cosmological background neutrinos (CNB) are thought to be a background relic which formed when the universe was about 1 second old. This background formed when the universe had expanded and cooled enough for neutrinos (and anti-neutrinos) to decoupled from the matter content in the universe [38, 39] and freely travel through it. Cosmological neutrinos have not been measured directly. The CNB energy scale is indirectly derived by looking at fluctuations in the cosmic microwave background of photons [40]. The anti-neutrinos denoted by BBN, are neutrinos produced by the decay of neutrinos and tritium during big-bang nucleosynthesis [41]. The next energy range is populated with thermal (anti-) neutrinos, and nuclear neutrinos that have been measured coming from

the sun (Solar) [42]. At slightly higher energies we find anti-neutrinos coming from nuclear reactors (Reactor) [4], or emitted by decaying radio active particles in the Earth (Geoneutrinos). The diffuse supernova neutrino background (DSNB) is a theoretical population of (anti-) neutrinos originating in supernovae. It is thought that this gives a continuous flux of neutrinos. Not to be confused with a single supernova event, which is thought to eject a huge amount of neutrinos in a burst. Unfortunately only one such event (SN1987A [22, 23]) has been measured. The next energy scale is associated with atmospheric (anti-)neutrinos. Atmospheric neutrinos are created when cosmic rays interact with the Earths atmosphere and generates a flux of secondary particles [43, 44]. These secondary particles consist of electrons which are absorbed in the atmosphere, muons which travel up to several kilometers into the Earth, and neutrinos which will travel almost undisturbed through the Earth. In section 3.1 we will briefly discuss the effects of atmospheric neutrinos and muons on our analysis. Atmospheric neutrinos are partially overlapping with the part of the spectrum we want to probe using the IceCube data.

For this work we will focus on neutrinos detected by the IceCube detector [30]. Part of the neutrinos detected by IceCube are thought to originate in cosmic sources such as, Blazars [33], and GRBs. We go into more detail on the detector in section 3.1. The highest energy neutrinos are thought to come from high energy protons interacting with the cosmic microwave background (Cosmogenic) [39].

2.3 Gamma Ray Bursts

Gamma Ray bursts (GRB) are very short intense flashes of gamma radiation. In a matter of seconds energies between roughly $10^{51} \sim 10^{53} \text{ergs}$ is emitted [46]. This is as much energy as the sun will produce in its entire lifetime. The initial gamma radiation burst, consists of photons with energies typically ranging roughly from a few keV to MeV , with some rare events at GeV energies. The initial gamma radiation burst, an afterglow is often observed. This afterglow consists of longer wavelength radiation in the radio [47], optical [48] and X-ray bands [49]. The bursts are relatively rare and occur about once every million years per galaxy. [50]. GRBs were first detected in 1967 by the Vela satellite system, which was intended to monitor the Nuclear Test Ban Treaty. In 1973 Klebesadel and Olsen [51] had found a total of 16 Gamma ray bursts of cosmic origin with a duration of up to 30 seconds. When in 1991 the Compton Gamma Ray Observatory launched its Burst and Transient Source Explorer (BATSE) it be-

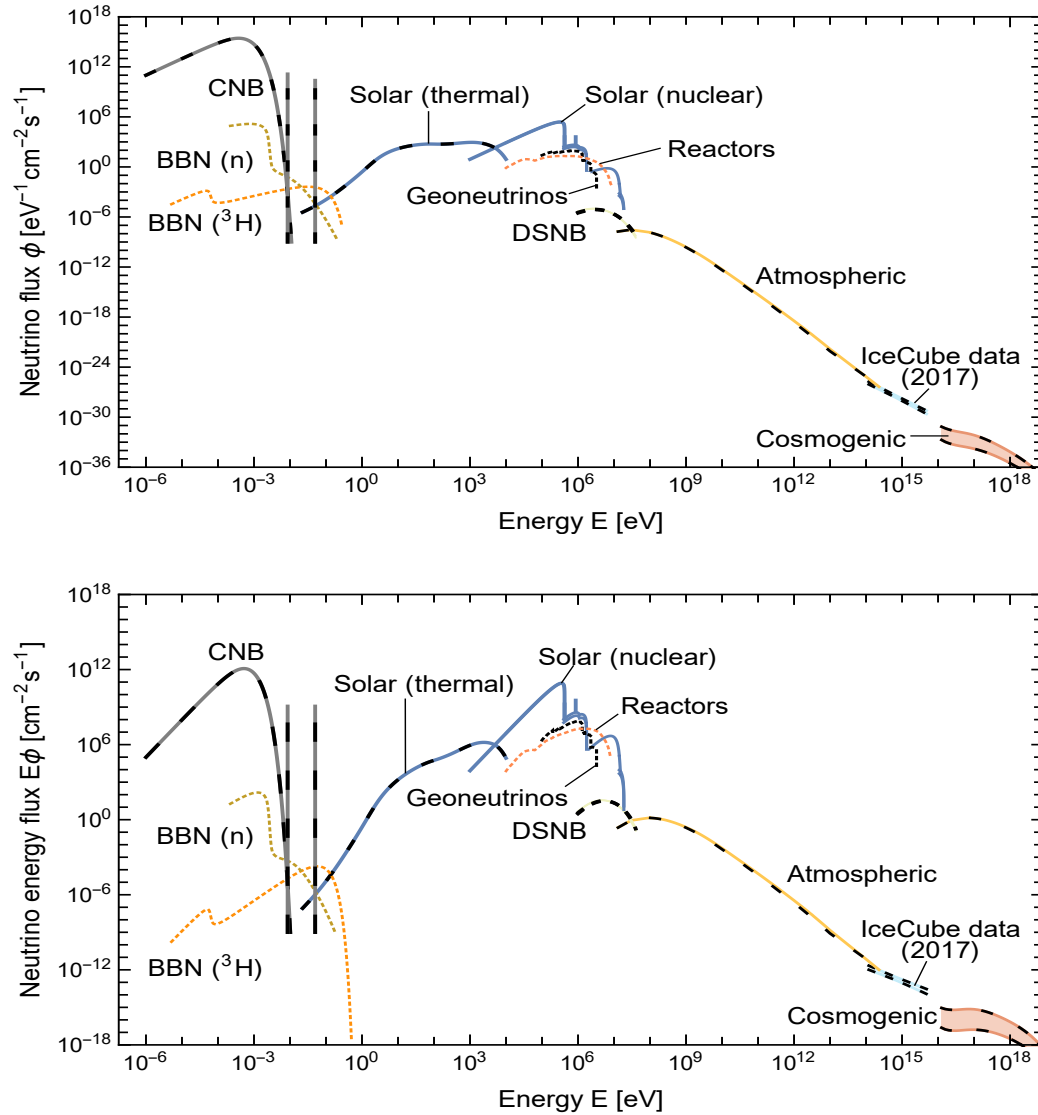


Figure 2.1: The top panel shows the measured and expected neutrino flux and energy for neutrinos from different sources. The bottom panel shows the flux times the energy. The spectrum is integrated over all directions and summed over all flavors. Solid lines are for neutrinos and dashed lines are for anti neutrinos. Superimposed solid and dashed lines are for sources that emit both. See the text for a per source explanation [45].

came possible to pinpoint to the GRBs location with more precision. This showed an isotropic distribution suggesting that most GRBs occur outside of the milky way [52]. Measuring the redshift of GRB970228 in 1997 by van Paradijs [53] further indicated the cosmic origin of GRBs. Since the first results from BATSE many more detectors, such as Fermi [54–56], and SWIFT [57, 58], have been collecting data on GRBs. This resulted in almost daily measurements of a new GRB. Data from all these bursts is collected and distributed by the Gamma ray Coordinates Network (GCN) [32]. We will be using data from the GRBweb, which is a GRB catalog maintained by [31]. We supplemented this data with information obtained from the GCN. GRBs have been measured coming from galaxies with a redshift of up to 9.4 [59]. The big distance from Earth and brightness of the measurements suggests that GRBs are hugely energetic events.

Due to all the effort of finding new GRBs a huge variety of GRB properties is found. This makes explaining the physics of GRBs a complicated matter. For GRBs that last long (on average 30 seconds) the most accepted model is the collapsar model [46]. This associates a burst with the death of a massive star followed by the formation of a black hole. The material that is falling into this black hole from the outer regions of the collapsed star can drive a pair of jets. The jets in turn can cause relativistic shocks, accelerating charged particles, in the media surrounding the black hole. This media contains electrons, photons but also baryonic matter [27, 60]. As soon as an electron reaches the edge of the star it is thought to emit photons through inverse Compton scattering. It is this burst of photons that is seen as a GRB. There are also thought to be protons in the accelerated media. They will interact with the photon field and result in high energy neutrinos.

It is thought that shorter duration GRBs (on average 0.3 seconds) can be caused by the merging of two compact objects like neutron stars, or a black hole and a neutron star [61]. The result of this merging is again the formation of a black hole which can form jets and radiation in the same way as the long bursts. These bursts can also occur far outside star forming regions and at lower redshifts than the long bursts we have discussed before [62]. Both the short and long duration GRBs eject a lot of energy in the form of gamma radiation and are expected to eject high energy neutrinos as well.

Observations

3.1 IceCube

As mentioned in section 2.2 neutrinos can travel long distances through dense clouds of matter without interacting. This makes it complicated to detect them. The general approach to detecting neutrinos is using a large volume filled with photo sensors that register light patterns in this volume that are caused by particles created in neutrino interactions.

In this analysis we will use neutrino events measured by the IceCube detector. This detector consists of a 3D array of photo-sensors submerged in a cubic kilometer of ice. The array of photo-sensors is used to detect light patterns in the ice. The sensors are incorporated in Digital Optical Modules (DOM) that send the detected light to the laboratory at the surface as a digital signal. A schematic overview of the detector as published by the IceCube collaboration is given in figure 3.1. The ice contains 5160 DOMs that are arranged on vertical strings with 60 DOMs per string. They are placed at a depth ranging from 1450m to 2450m and separated by 17m vertically and roughly 125m horizontally. The detector has been collecting data since before it was completed. The different configurations of the detector are referred to by the number of strings that were actively collecting data. For this thesis we will use public data collected when IceCube was in its 40, 79, and 86 string configuration, which we will refer to as IC40, IC79, and IC86 respectively. Apart from using the deeper regions of the Ice to detect light the detector also has a top layer, called IceTop. This layer is used to calibrate the detector. It can detect air showers coming from cosmic rays with an energy from 300TeV to 1EeV. In the center of IceCube lies a region with the strings closer together. This region is called the DeepCore, and is used to investigate lower energies [63].

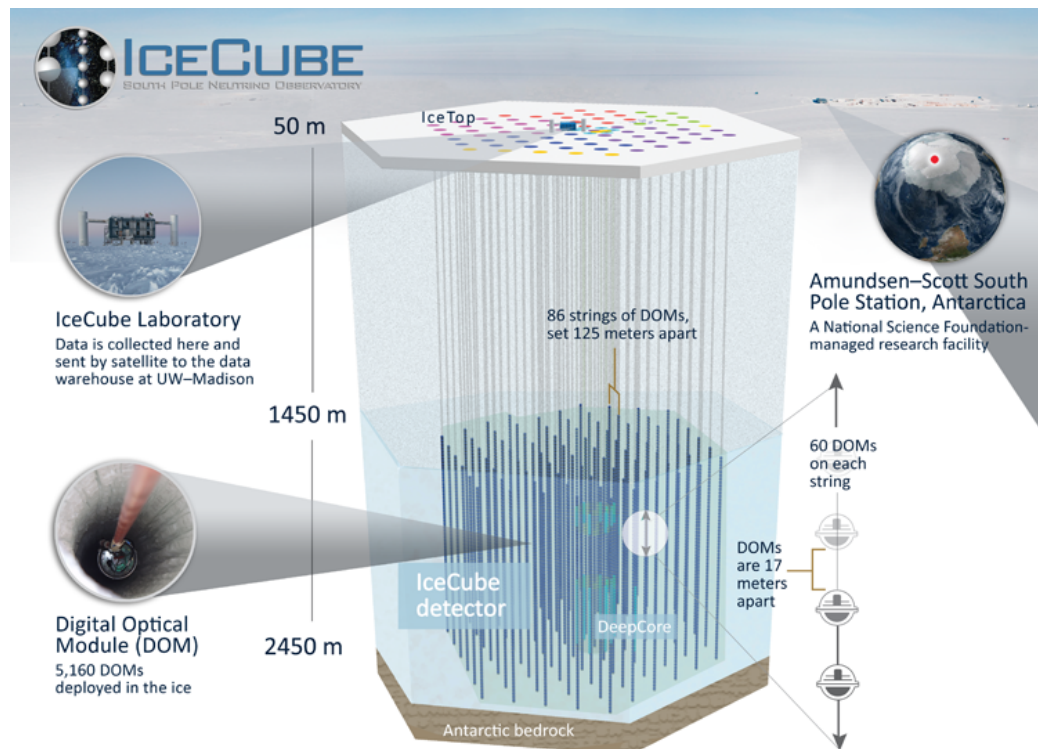


Figure 3.1: A schematic overview of the IceCube detector as published by the IceCube collaboration.

IceCube cannot detect neutrinos directly. Instead it detects light caused by particles that are produced by the interaction of a neutrino with the ice. When a neutrino interacts with the ice it produces electrically charged particles. These particles travel through the ice faster the light travels through ice. As a result the particles cause Cerenkov light. This can best be explained as a light shock wave that follows the particles path similar to a sonic boom following an aircraft flying at supersonic speed.

The IceCube detector can detect three different types of neutrino events. There can be cascade- or shower-like events, which are created by charged current interactions of electrons or tau neutrinos, or by neutral current interactions of any type of neutrino. Figure 3.2a shows an example signature that an electron neutrino leaves in the detector. These type of events can be reconstructed with a median angular resolution of about 10° . Due to the large amount of scattering of the light they produce almost spherically symmetric signal in the detector.

IceCube has also detected the atmospheric tau neutrino interactions [64]. Due to the short lifetime of the tau lepton it can decay in another

cascade after a short distance. These cascades can both contain charged particles and be visible in the detector.

For our work we will be using track like events. The track like events are caused by muons. Muons are created in charged current neutrino interactions in the ice or atmosphere. As a muon travels through the detector ice it will leave a trace of Cerenkov radiation pointing to the direction it came from. Due to the long track like signal the muon causes in the detector it is possible to point to their origin with a reconstructed angular resolution in the order of 1° [65]. The good angular resolution is useful for studying far away objects because it points to the location with more precision than can be done using cascade like events. An example of a muon signature is given in figure 3.2b. Another reason for choosing the track like events caused by muons is their great abundance. They cannot only be detected if a neutrino interacts with the ice to form a muon, but also reach the detector if such an interaction has occurred in the sky outside of the detector.

To probe the neutrino energy of a detected event we have to be careful. The IceCube collaboration has not published an error estimate on the observed energies. Instead they warn users users that the energy is derived from looking at the energy loss of a muon, as it travels through the detector [63, 66]. For this reason they suggest using it as a lower estimate of the neutrino energy with a reconstruction error of roughly 30%. An extra complication for gathering neutrino data from muons is that most of these events measured by the detector will be muons resulting from cosmic rays interacting with the Earths atmosphere [67]. These type of events are called atmospheric muons and flood the detector with roughly 10^{11} events per year [64]. One method of removing an atmospheric muon signal from the data uses the Earth as a blocking filter. When an atmospheric muon travels through the Earth it will interact with the particles in the Earth and not reach the detector. There does however exist the possibility to wrongly reconstruct the neutrinos direction and mistake an down-going neutrino for an up-going one. The IC 40 data for example only contains up-going neutrinos. This simplifies our analysis but at the same time removes half the neutrino information the detector can collect.

3.1.1 IceCube neutrinos

We have shown in section 2.2 that neutrinos can be produced in many different sources. Depending on the source we expect them to have a different energy spectrum. It is important to note that the energy dictates

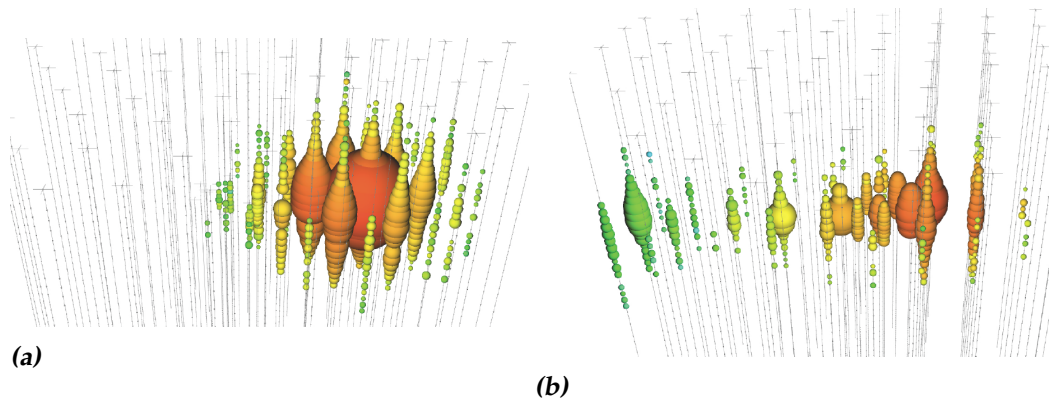


Figure 3.2: A cascade signature of an electron neutrino as registered by IceCube in figure 3.2a and a track like signal from a muon that is created as a secondary particle by a muon neutrino in figure 3.2b. The colors denote arrival times of light in the Doms, from earlier (Red), to green to blue (later).

how likely a neutrino is to interact. To detect a neutrino we need it to interact with matter close to the detector. Neutrinos interact almost purely through the weak force. We want to know how the probability of such an interaction depends on the energy. The interaction probability is described by the cross section. It is given in units of the area transverse to the relative motion of two particles, within which they must be in order to interact. Many works have been published on the cross section of neutrinos, see for example [68, 69]. For neutrino interactions, its cross section increases with its energy. This means that a higher energy neutrino is more likely to interact with the medium it is traveling through than a low energy neutrino. The highest energy neutrinos will not even reach the detector when they have to cross the Earth.

To set up our analysis we follow the same method as used in [28]. We apply it to the IC40 data [30] so that we can validate our implementation with the analysis of [28] of the same data. Since IceCube will detect a lot of atmospheric muons and we are not interested in those a filtering choice is made. Atmospheric muons can not travel all the way through the Earth, so by selecting only events going up in the detector we remove most of the atmospheric muons. The IceCube detector is located at the south pole. This means that all the up-going events in the IC40 data are all coming from the northern hemisphere. By selecting this part of the data we have used the Earth as a filter that blocks the atmospheric muons from reaching the detector. Unfortunately some atmospheric muons will be reconstructed wrong and also look like up-going events. This method

removes at least most of the atmospheric neutrinos. We will be looking for neutrinos that can be associated with GRBs. We will discuss in section 2.3 that these sources are isotropically distributed over the sky and are not observed with any specific timing profile. It is therefore useful to confirm if our neutrino data follows the same overall distribution. In figure 3.3 we have shown the detection time and spatial distribution of the neutrinos in the IC 40 data. We see that the neutrinos are distributed isotropically over the space. In the next section we will take a look at the GRB data we have compiled. We also make a selection of the GRB data we will use for correlating with neutrino data.

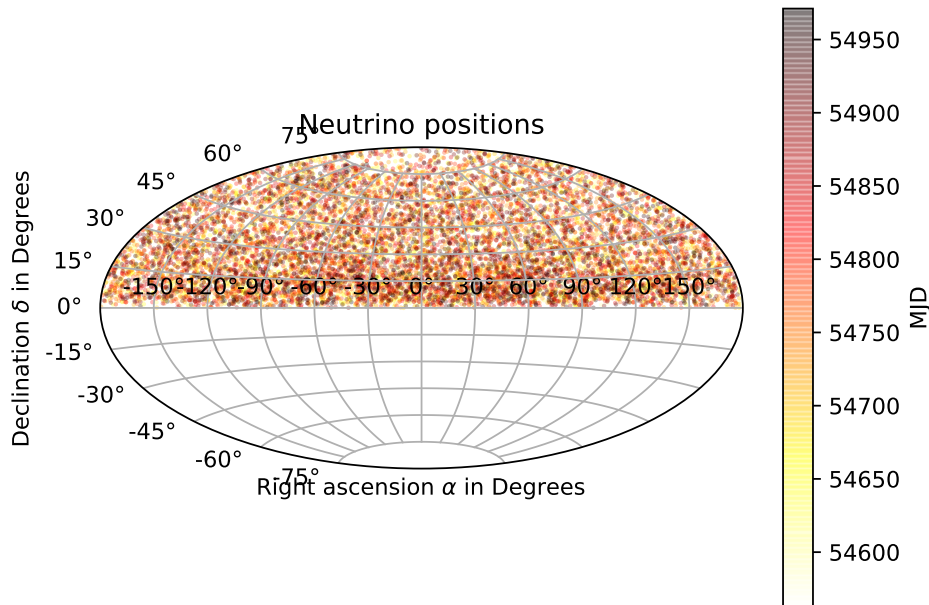


Figure 3.3: The distribution of 12875 neutrinos on the sky in equatorial coordinates as measured by IceCube in its 40 string configuration. The colors denote the time in Modified Julian Date of the measured event.

3.2 Gamma Ray Burst observations

To be able to explore potential LIV in GRB neutrinos a data sample of GRBs is required. We have used GRB information obtained from GRBweb

[31]. We also supplemented the GRBweb data sample with bursts obtained from the GCN network [32] to find a total of 5344 bursts. The equatorial positions of the GRBs can be seen in figure 3.4. The colors in this plot denotes the Modified Julian Date.

In section 3.1.1 we looked at neutrino data that was already analyzed by J. Schmid [28]. To repeat her analysis we will need a set of GRBs to compare to the neutrinos. Unfortunately she only published the GRBs that were compared to Antares neutrinos and not to IceCube neutrinos. So we will not be sure of her exact data. When comparing the GRBweb catalog to her published table we did however find some bursts missing in the GRBweb, or in her tables. We contacted the maintainer of the GRBweb page, who could then update his code to include at least part of the missing bursts.

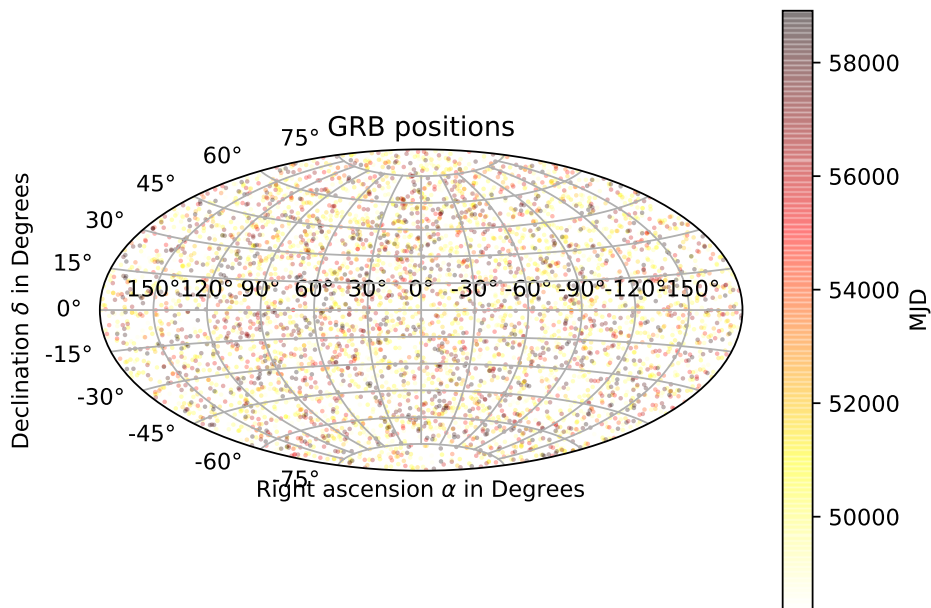


Figure 3.4: The distribution in equatorial positions of all 5344 GRBs [31, 32]. Colors denote the Modified Julian Date.

3.2.1 Gamma Ray Bursts for IC40

Since our goal is to relate the neutrino and GRB data we should first consider if the data was taken from the same part of the sky, and during the same period. The IC40 data sample consists only of neutrinos coming from the northern hemisphere. This means that we cannot associate it to any GRB that is in the southern hemisphere. We follow the declination boundary of IC40 and drop all GRBs that have occurred with a declination of $\delta \leq -5^\circ$. Next we can consider during what time period the data was collected. The IC40 data was collected from April 2008 to May 2009. We want to associate neutrinos to GRBs that have occurred within a certain time window around a GRB. We define the time window in section 4.2.2. In order to be sensitive to the entire time window we remove all bursts for which the chosen time window is not fully included in the time period of neutrino data taking. This will ensure that we do not find any preferred time difference between a neutrino and its associated GRB, purely due to our data taking periods. In section 3.1 we discussed that the events observed in the IceCube detector contain a large background consisting of atmospheric neutrinos, and even some wrongly reconstructed atmospheric muons. To decrease this background we do not want to associate neutrinos with bursts that might have occurred in a big positional search cone. In figure 3.5 we see that the observed GRB error can go up to $O(10^\circ)$. Using such a big positional search cone would lead to diluting the potential high precision neutrino to GRB associations with a large amount of lower precision events. Instead, we set the maximum allowed positional error of GRBs at δ_{err} and drop all bursts with bigger error from our sample.

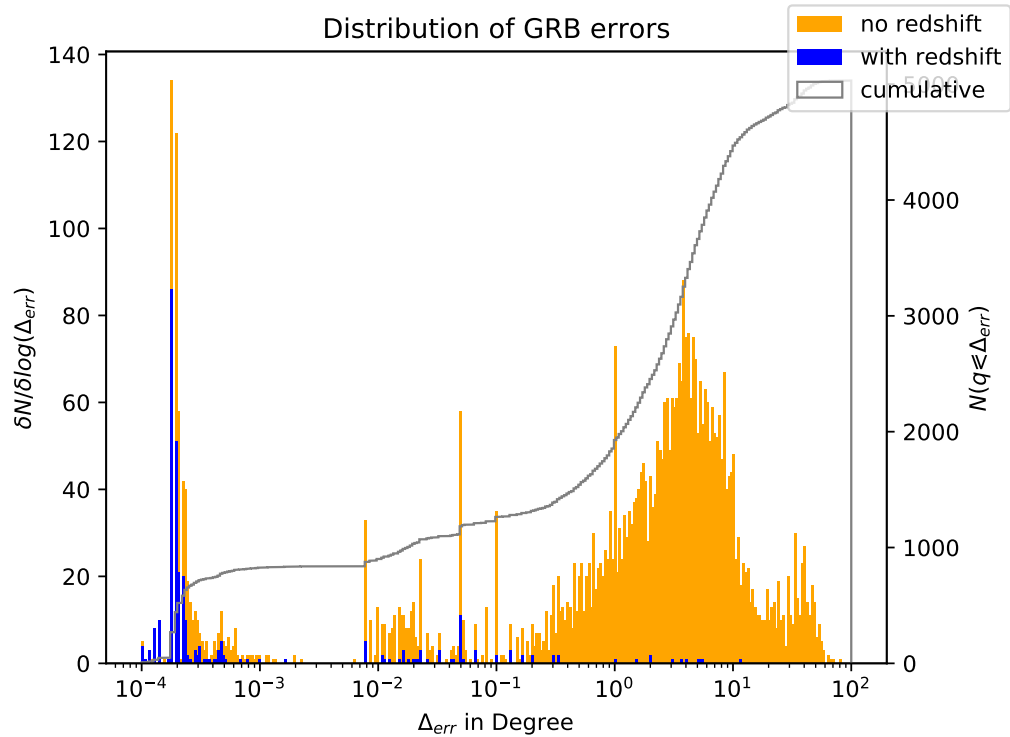


Figure 3.5: The distribution of the GRBs positional errors [31, 32]. The blue bars denote GRB's for which we have a redshift measurement. The orange bars correspond to bursts without a redshift measurement. The gray line gives the cumulative distribution of the positional errors.

The spatial distribution and time of the selected GRBs can be seen in figure 3.6. In table 3.1 we have summarized how the number of GRBs changes for each new selection criteria. The distribution of the selected GRBs positional errors can be seen in figure 3.7. By making this first selection our sample has been reduced to 58 GRBs.

Variable	Criterion	N_{effected}	N_{total}
N_{GRB}		0	5344
δ_{err}	$\leq 3^\circ$	2176	3168
δ	$\geq -5^\circ$	1558	1610
MJD	$\in [54602, 54931]$	1552	58
redshift	any	41	17

Table 3.1: The number of GRBs using different selection criteria. N_{effected} is the number of GRBs effected by a criterion, and N_{total} is the total number of GRBs left after applying the criteria in order.

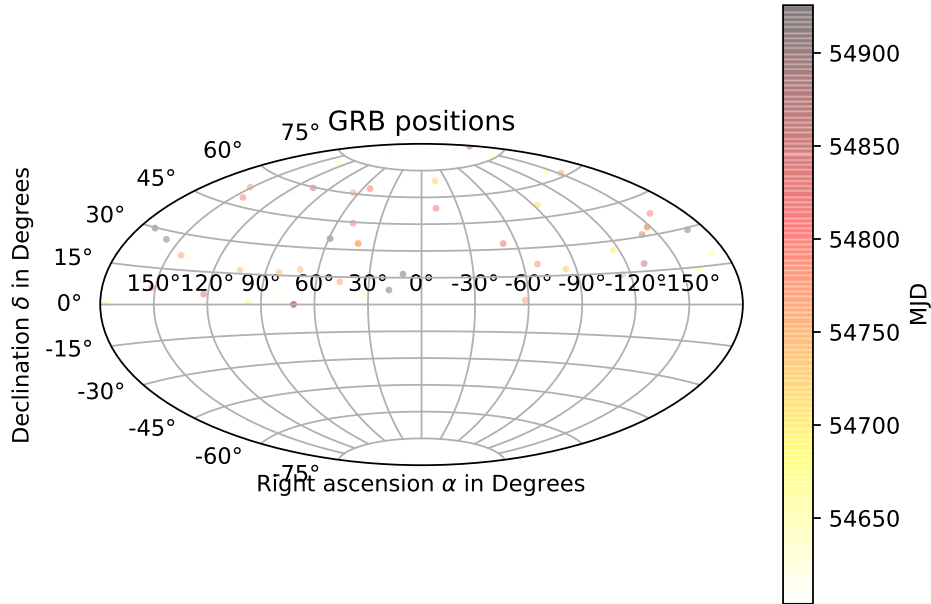


Figure 3.6: The distribution of 58 gamma ray bursts, in equatorial sky coordinates, present in the catalog after we have used all the sampling criteria in table 3.1. The colors denote the time in Modified Julian Date of the measured event.

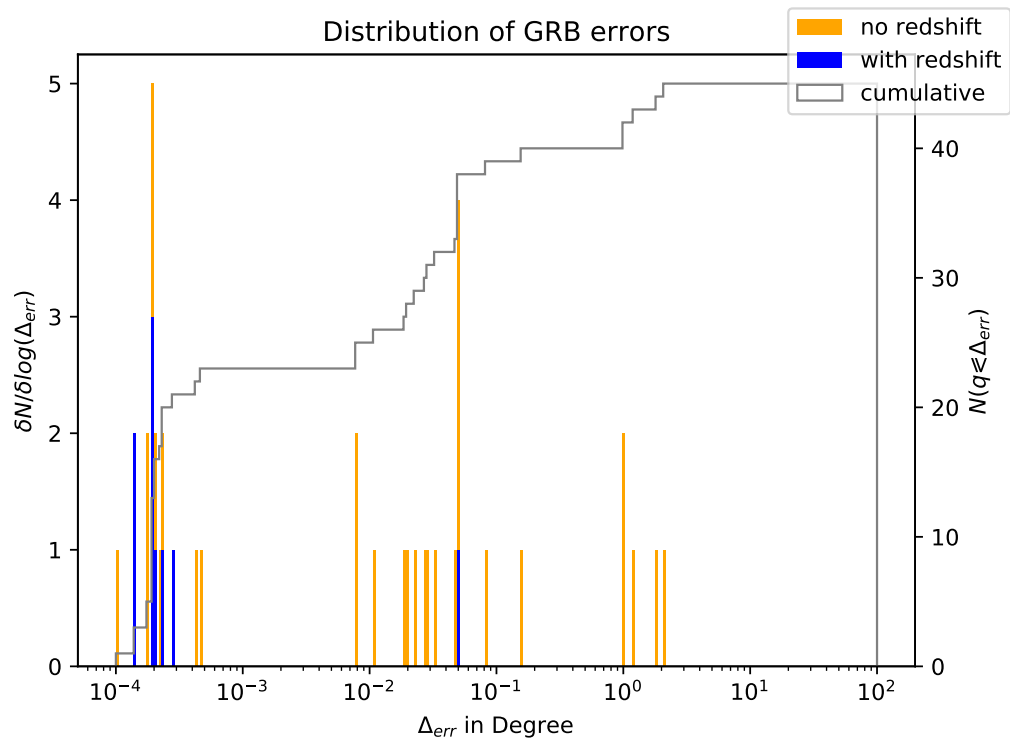


Figure 3.7: The distribution of GRB positional errors with redshift (blue), and without redshift (orange). The cumulative distribution is seen in gray.

Method

We set out to look for observed time differences, Δt_{obs} , between photons and neutrinos that are emitted by the same GRB. We want to use these time differences as a probe of Lorentz violation. However, much is still unknown about the physics of GRBs. We are for example not at all certain that a GRB emits photons and neutrinos simultaneously. It is possible that there is an intrinsic time difference, Δt_{in} , present between the emission of a neutrino and a photon. Furthermore we have to take into account that a signal that is emitted at one time will be redshifted by the time it reaches an observer at Earth. In equation 4.1, the relation between the different times used in this study given.

$$\Delta t_{obs} = t_{LIV} + (1 + z)\Delta t_{in} \quad (4.1)$$

We have already given an expression for t_{LIV} in equation 2.2. Combining this with equation 4.1 leads to a formula for the observed time difference over the redshift. Note that we have followed [34, 36] in assuming that the neutrinos energy is much bigger than that of the photon, and hence dropped the photon energy from this formula. We can determine what time differences we expect to find for neutrinos of known energy if we make assumptions on the size of Δt_{in} and E_{LIV} .

$$\frac{\Delta t_{obs}}{1 + z} = \pm \frac{E_{\nu}}{E_{LIV}} \frac{D(z)}{c} + \Delta t_{in} \quad (4.2)$$

Since the LIV effects can possibly delay or advance the arrival times of neutrinos with respect to photons we have to account for both situations. The minus sign is used if the neutrino signal is delayed with respect to the photon, and a plus sign if the neutrino signal is arriving earlier. In the end the signals we can probe will be the arrival time differences of GRB

t_ν		Observation time of neutrino on Earth
t_{GRB}		Observation time of GRB on Earth
τ	$t_\nu - t_{GRB}$	Observed time difference on Earth
τ_z	$\tau/(1+z)$	Time difference corrected for redshift
τ_{LIV}	$\tau/(E_\nu \cdot D(z))$	Time difference due to LIV

Table 4.1: Different time measurements used throughout this work.

neutrinos and their associated photons, the redshift to a GRB, and neutrino energy. From these observables we can construct three different time difference measurements. An overview of these measurements is given in table 4.1. Here $\tau = t_\nu - t_{GRB}$ probes the observed time difference on Earth. We can use $\tau_z = \tau/(1+z)$ as a probe of the intrinsic time difference. This boils down to correcting our observations for the redshift. If Lorentz violations are present we can best probe those by using $\tau_{LIV} = \frac{\tau}{E_\nu D(z)}$. We have shown in equation 4.2, that the observed time difference in the presence of LIV depends on the neutrino energy and the distance to the source. For this work we follow [28, 34, 36] and assume that the intrinsic time difference in neutrino and photon emission is always the same. It is important to note that a lot is still unknown about GRB physics, so this could be a wrong assumption. There might be for example a correlation between neutrino energy and intrinsic time shift, that we have omitted by making this assumption. If we find a specific preferred value of τ_{LIV} , this would indicate the presence of an effect compatible with LIV. We expect to see these effects more clearly for higher energy neutrinos, since then $t_{LIV} \gg \Delta t_{in}$, for PeV neutrinos and an E_{LIV} is of the order of 10^{18} GeV [34].

As we have seen in figure 3.7 the redshift is only known for about 10% of the GRBs. This means that we will only be able to use a small fraction of the GRB measurements when considering possible time shifts. To have an overview of the difference in arrival times we will stack all the time differences of neutrinos and the associated GRB in a single histogram. If there is a LIV effect we expect there to be a significant peak in this histogram. A complication to this approach comes from the fact that we do not know if a neutrino truly comes from a GRB source. To distinguish a background signal from a cosmic signal we follow the statistical approach explained in section 4.1. Using pseudo experiments, as given in section 4.3, we simulate both signal and background. From this we can derive ‘stacked’ or ‘cumulative timing profiles’ for each hypothesis. Using these profiles we are able to distinguish signals of different strengths compared

to background. We define when there is a correlation or 'match' between a neutrino and a GRB in section 4.2. In the next sections we follow the statistical approach used in [28] and apply it to the data introduced in chapter 3.

4.1 Statistical approach

One of the challenges of using neutrino data in multi messenger astronomy comes from the abundance of background events in the observed data. We set out to find GRB neutrino sources, which we will call our signal. To search for an excess of signal over the background we will use the goodness of fit test, developed by [70]. This method aims at quantifying the compatibility of observations with a hypothesis. In the case of cosmic neutrino search, we can test how well our data matches the null hypothesis: "None of the observed neutrinos are produced by Gamma Ray Bursts". If the data does not match the null hypothesis with a high enough degree of incompatibility, we reject the null hypothesis. We can also consider how well our data compares with an alternative hypothesis. For example: "Some neutrinos originate in gamma ray bursts". Since we do not want to make assumptions about the physics of GRB sources we can not formulate the alternative hypothesis in such a way that we can differentiate with high certainty between the null and alternative hypothesis. All we can find is the degree in which our data matches one or the other hypothesis.

4.1.1 Goodness of fit test

The goodness of fit test is used to study the compatibility between our measurements and a given hypothesis. We will do this in terms of a test statistic, ψ . This test statistic can be any function of the experiments observables. It is constructed in such a way that it allows for distinguishing a systematically time shifted signal from the cumulative timing profile corresponding to a hypothesis. For this we will need to know how our timing profile would look if the hypothesis is true. For the null hypothesis this means that we have to find a data sample consisting of only uncorrelated events. We do not a priori know what part of our data can be considered background and what part can be considered signal. Instead, we can use pseudo experiments to generate data that is used as a possible realization of uncorrelated neutrino data. This is done in section 4.3. The p-value is calculated by comparing the observed value of the test statistic, ψ_{data} , to

the distribution of ψ under the hypothesis that we are testing. This quantity is defined as the probability to observe a value of ψ under the tested hypothesis, that is at least as extreme as ψ_{data} . We have shown an illustration of the goodness of fit test in figure 4.1. Here the black curve represents the probability density function (pdf) of the test statistic, ψ , under the null hypothesis. All the values of ψ under this curve are called the sample space. The vertical line denotes the value of the test statistic found from actual observations, ψ_{data} . The gray area gives all the values contained in the sample space higher than the value of ψ_{data} . The surface of this area corresponds to the one sided p-value.

We can also define when we will reject the null hypothesis. This is done by stating at what p-value our data is not compatible with the null hypothesis. This value is chosen so that it is unlikely to find a value of ψ_{data} , so large under the null hypothesis. This p-value is given by the red area in figure 4.1. It is bound by a threshold value, ψ_c . It is important to note that the threshold value is set by our choice. If we choose a very small threshold value, we increase the chance of falsely rejecting the null hypothesis. For this work we will assume that we find hints for rejecting a hypothesis when its p-value is smaller than $p_{3\sigma} \sim 2.7 \cdot 10^{-3}$. Here we have used the conventional notation, where $n\sigma$ corresponds to the number of standard deviations, σ , away from the normal distribution. $p_{n\sigma}$ is calculated from the two sided p-value under the normal distribution with standard deviation σ . This approach can be applied to study the compatibility of our data with hypotheses representing different physical scenarios.

Before using any data however, we can compare the null hypothesis with an alternative hypothesis. For this we will calculate the threshold value $\psi_{3\sigma}$, corresponding to $p_{3\sigma}$ from the background distribution. We can use this value to calculate our power at distinguishing a simulated signal pdf from the background pdf. We calculate the surface under the simulated signal pdf above the threshold to find the discovery power. This gives the probability to find a value $\psi_{alternative} \geq \psi_{bg}$. A larger the discovery power thus means that we can better distinguish the null hypothesis from the alternative hypothesis.

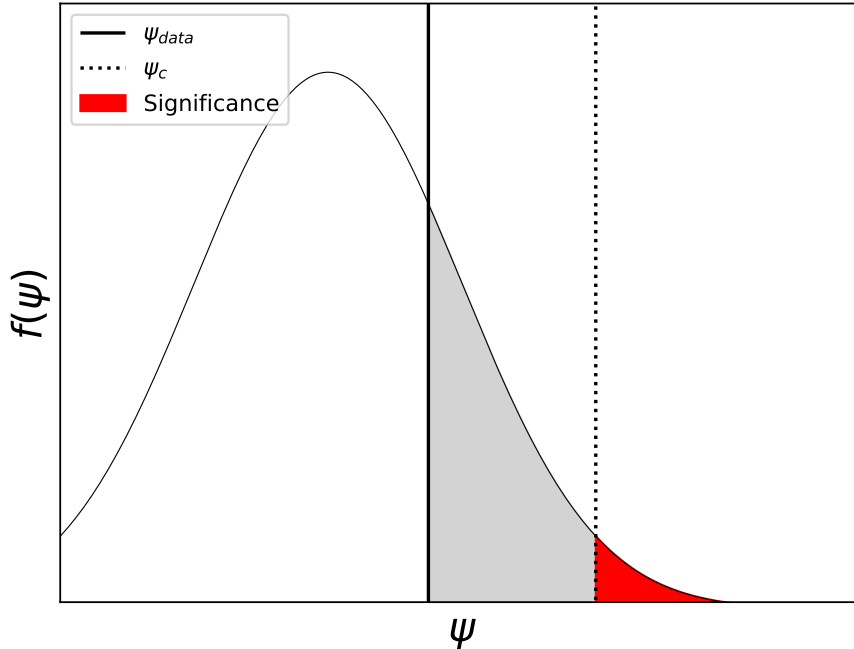


Figure 4.1: Schematic illustration of goodness of fit approach. The probability of finding ψ under the null hypothesis is shown as a function of ψ as black curve. The gray area corresponds to the p-value corresponding to observations. It is bound by hypothetical value ψ_{data} , that is represented with the vertical black line. The vertical dotted black line indicates the chosen threshold value ψ_c (see text), whereby the red area corresponds to the associated significance.

4.1.2 The test statistic

We introduced the concept of a test statistic in the previous sections. Now it is time to define it for the case at hand. We follow [28, 71, 72] and use a test statistic that allows for a way to evaluate the compatibility of our found timing profile and the background scenario, as described by the null hypothesis. We will describe our timing profile, and the background scenario, in terms of a histogram containing the number of matches per observed time difference. The observables that we will be using is thus the number of neutrino to GRB associations and the time differences of these associations. The probability to find an outcome of this experiment, A_k , is given by p_k . For successive trials of this experiment the probabilities are independent and stationary. This means that these experiments

belong to the Bernoulli class B_m [73]. We can now write the probability $p(n_1 \dots n_m | B_m, I)$, of observing n_k occurrences of each outcome A_k after n trials using the multinomial distribution.

$$p(D|B_m, I) = \frac{n!}{n_1! \dots n_m!} p_1^{n_1} \dots p_m^{n_m}. \quad (4.3)$$

Here D denotes the data realization spread out over m different bins. I is the prior information we have about the system. n_k denotes the number of events contained in a single time difference bin, k . We follow [28] and [71] in writing our test statistic as a logarithmic function of this probability. See appendix A for more information.

$$\begin{aligned} \psi &= -10 \log_{10} p(D|H, I) \\ &= -10 \left[\log_{10} n! + \sum_{k=1}^m (n_k \log_{10} p_k - \log_{10} n_k!) \right] \end{aligned} \quad (4.4)$$

The test statistic can be used as a reference to quantify our degree of belief in H . It is constructed of the total number of events, n , in our data, the number of events per bin, n_k , and the probability to find an event in a certain bin under the null hypothesis, p_k . Using the time difference binning means that we can include information on the observed time differences in our test statistic. In table 4.1 we have given three different probes for the time difference. For each of these probes we can find a timing profile from associating neutrinos to GRBs. The timing profiles give the number of matches with a certain time difference. For this we have divided the total time window into time difference bins, denoted by k . We define the bin width so that signals from different GRBs are isolated and the emission associated with a single GRB falls within one bin. The resulting timing profile of a the data will therefore be discretely distributed with roughly zero or one match per time difference bin. We can also use some prior information about the background scenario in defining our test statistic.

We know that the background scenario as described by the null hypothesis will not lead to any preferred time difference in the τ profile. This means that if we have m bins in total, the probability for a match to fall into a single bin is $p_k = 1/m$. For the other two timing profiles it is not so easy to find the background distribution of time differences. Instead, we can use the pseudo experiments described in section 4.3 to calculate the probability for a match to fall into a certain time difference bin. We expect this probability to be higher for lower values of $|\tau_z|$, and $|\tau_{LIV}|$, since we divide the time difference by values bigger than one. We calculate the pdf of the test statistic for each hypothesis using equation 4.4, which is the same as

in [28]. It is important to note that these properties depend on the choices made by the experimenter. The number of neutrinos we can associate to a GRB depends on our definition of a match or association. The number of bins we use depends on the size of the allowed time difference between a neutrino and a GRB. In the next section we will discuss the matching criteria in more detail.

4.2 Matching criteria

We are looking for neutrinos that can be associated with a GRB. This means that we expect the GRB measurement and the neutrino measurement to align in both position and time of occurrence. Since the measurements both have an error we have to define a certain criteria that specifies when a neutrino matches to a GRB. For the time matching we have to be even more lenient since we want to look for a time shift due to LIV effects. It is important to note here that we expect tighter constraints on the matching criteria to increase the ratio of signal to background. Setting the constraints too tight however will result in also removing signal from our data. To find an optimum choice we will use some physical considerations, but have to keep this in mind too. Below are the considerations on the search cone size and time window we will use for matching neutrinos to GRBs. To allow for comparison to literature we used the same criteria as in [28].

4.2.1 Search cone size

We will first set a criterion for spatially matching neutrinos with GRBs. A neutrino is potentially originating in the same event as a GRB when it is measured within a certain distance from the GRB. We are effectively looking in a search cone centered around a GRB source. The size of this search cone can be set depending on the positional error in the GRB and neutrino measurement. As can be seen in figure 3.7 the error in the GRB measurement can take many different values. The neutrinos however do not have a per event error measurement in the IC40 data. Instead, we can use the median angular resolution derived from Monte Carlo simulations in [30, 74]. This simulation was done with the same reconstruction quality criteria as the original data consisting of 12877 neutrinos. A resolution of 0.7 degrees is derived. An obvious choice of search cone radius, δ_{cut} , would be equation 4.5.

$$\delta_{cut} = \sqrt{\delta_v^2 + \delta_{GRB}^2} \quad (4.5)$$

Here δ_ν is the angular resolution of the neutrino data and δ_{GRB} is the positional error of the GRB we are considering. Since there are a lot of GRBs with a large positional error, as shown in image 3.5, we will also have a lot of big search cones to consider for coincidences. This will lead to more matching neutrinos, but also dilutes the possible signal with background matches. On the other hand for the smallest positional errors reported in the GRBweb catalog the search cone size will be dominated by the resolution of the neutrino telescope. Since this is based on the median angular resolution and not on the per event error, this might lead to removing potential matches between neutrinos and GRB photons. To account for these effects we follow the suggestion by Julia Schmidt and the Antares collaboration [28, 29] and limit the size of the search cone using equation 4.6. This equation is designed, in [28], to find a search cone at least bigger than the neutrino resolution, but smaller than 3 degrees to not dilute a possible signal too much.

$$\delta_{cut} = 1.58 \cdot \max(\delta_\nu, \min(\delta_{GRB}, \delta_{err}^{max})) \quad (4.6)$$

To keep the search cone under three degrees a maximum error is introduced of the size $\delta_{err}^{max} = 3/1.58$. Using the 0.7° reconstructed resolution of the IceCube data as a minimum of the search cone size we find $\delta_{cut} = 1.1^\circ$. We follow the formulation of [28] and introduce the factor of 1.58. There this factor is used to optimize for the signal to background ratio in a high background scenario. Since we will eventually compare our results to that in [28] we follow the same convention.

If in the future the positional errors are defined precise enough for neutrinos too it will be interesting to combine equations 4.5, and 4.6. The logic of squaring the errors to find a new search cone size is more intuitive, while limiting the search cone size restricts the background contamination. I suggest using equation 4.7 in future works. This limits the search cone again to a range of 1.01 to 3 degrees, and also takes into account the neutrino and GRB error measurement, instead of picking the biggest of the two.

$$\delta_{cut} = 1.58 \cdot \sqrt{\min(\sigma_\nu^2, \Delta_{err}^{max}) + \delta_{GRB}^2} \quad (4.7)$$

4.2.2 Time window

Now that we have set some boundaries on the search cone size we should look at the maximum time difference we expect to see for a neutrino-GRB pair. To decide on the size of the time window we want to consider around

each GRB we can use equation 2.2. We see that the time shift depends not only on the LIV effect but also on the neutrino energy and the distance to the source. Previously time windows of the order of -1 to $+3$ hours [75], and from 10 seconds all the way up to 15 days [76] have been studied without finding any significant GRB to neutrino association.

In later works a LIV shifted signal was derived at a LIV scale of $E_{LIV} = (6.4 \pm 1.5) \times 10^{17} \text{ GeV}$, by allowing for a time window of up to 40 days [34, 36]. We will use the same sized time window in this work to allow for comparison. The choice of such a large time window size is justified in [28] by considering what the biggest observed time difference due to LIV effects can be. For deriving the maximal time shift we can use the values in the IceCube data taken between April 2008 and May 2009 and the GRB data that complements this. In equation 2.2 we have shown that the LIV time shift depends on the neutrinos energy and the distance to a source. As in [28] we used the distance at a redshift of $z = 8.5$, which is the highest redshift in the GRB data, and $E_{max} = 10^9 \text{ GeV}$ accounting for the energy range at which a signal might be observed by IceCube. We also have to use an estimate on the LIV scale to derive the maximum time window. We follow the suggestion in [28], and use $E_{LIV} > 7.6 \cdot M_{Planck}$ as limit on on the LIV scale. This value is derived from FERMI/LAT data by [17]. We now find a maximum time window of ± 470 days. Since this time window is larger than our neutrino data taking time for the IC40 sample we cannot use this. Instead, we assume a smaller maximum value for the neutrino energy of the order of 10^8 GeV . This is still much higher than the highest observed event in our data, which has an energy of $0.32 \cdot 10^6 \text{ GeV}$. The neutrino energy supplied by the IceCube collaboration should be treated as a lower boundary with high uncertainty as mentioned in section 3.1. We now find a time difference of closer to the previously used ± 40 days. To compare our work with previous studies [28, 34, 36] we will stick to the 40 day time window.

As a last remark we should again consider the number of bins used in the stacked timing profiles. We want the signal associated to different GRBs to be distinct in the time difference histogram. In section 4.4.1 we will show that we expect to find $O(3)$ events per GRB, for a total of 58 GRBs. This means that if we use timing bins of roughly 13 hour we expect the signal to be discretely distributed with approximately one or zero events per bin, for each data realization.

4.3 Pseudo experiments

The null hypothesis is defined as: "None of the observed neutrinos are produced by Gamma Ray Bursts". To be able to compare our observations to this hypothesis we want to know what a neutrino background looks like. Going back to figure 3.3 we can already see that the neutrino distribution is roughly isotropic. Even after filtering out atmospheric muon events we are still left with a lot more neutrinos than GRB sources (figure 3.6). A part of the neutrino events can be associated with a GRB but we will not know whether these are background neutrinos or GRB neutrinos. To approximate a background distribution of the test statistic, ψ_{bg} , without signal we will use pseudo experiments. These pseudo experiments consist of generating possible realizations of neutrino data by randomizing their detection times and positions. In section 4.3.1 we will explain how we have randomized the data precisely. For now it is enough to know that we can use the randomized data to look at the time differences between a neutrino and an associated GRB. For each pseudo experiment we find a new time difference distribution, or timing profile. We repeat this process many times over and calculate a value of the test statistic for every realization. This gives us an approximation of the background distribution of neutrino to GRB associations. Any signal that might have been present in the original data is removed by the randomization while the background profile still follows that of the original data.

We can also generate data for an alternative hypothesis. Even without knowing much of the physics behind the system we can assume that a certain amount of signal is present. For example: "10% of all Gamma Ray Bursts have emitted an observed neutrino". To test our data against this hypothesis we have to find the pdf of ψ for the alternative hypothesis. We can again compare this to our chosen threshold value and see how well we can distinguish two possible hypotheses. We create a possible realization of the neutrino data just as was done in the background scenario. This time however, we inject known signal in the neutrino data. In section 4.3.2 we explain how exactly we injected a neutrino signal. We follow the same logic as for the background scenario and end up with a profile of a randomized background. This time however, it also contains an excess of neutrinos correlated to GRBs.

4.3.1 Simulating background

For the IC 40 neutrinos we can define a few possible scenarios. We want to test our data against the null hypothesis first. It is also interesting how

it compares to an injected signal of matching neutrinos. We consider the same cases as in [28] to allow for a cross check. For the background scenario we want to generate pseudo pseudo experiments of uncorrelated neutrino data. We have shown in figure 3.3 that the detected neutrino events follow an isotropic distribution in both time and space. In section 5.1 we will see that the the detectors efficiency at detecting events depends on the events energy and its declination. This effect will still be present in a background distribution. From figure 4.2 we see that the right ascension of an event does not have a preferred direction. This means that we can use both time and right ascension randomization to generate a background distribution. To do this, we first scramble the measured neutrino arrival times. Then we use the new arrival time to calculate how much we have shifted the neutrinos time of observation. We can then use this time shift to calculate a new position for the source in equatorial coordinates. Since the IceCube detector is located at the south-pole we do not expect the declination to change significantly. We can thus calculate the new right ascension by moving the events incident direction at the same speed as the rotation of the Earth.

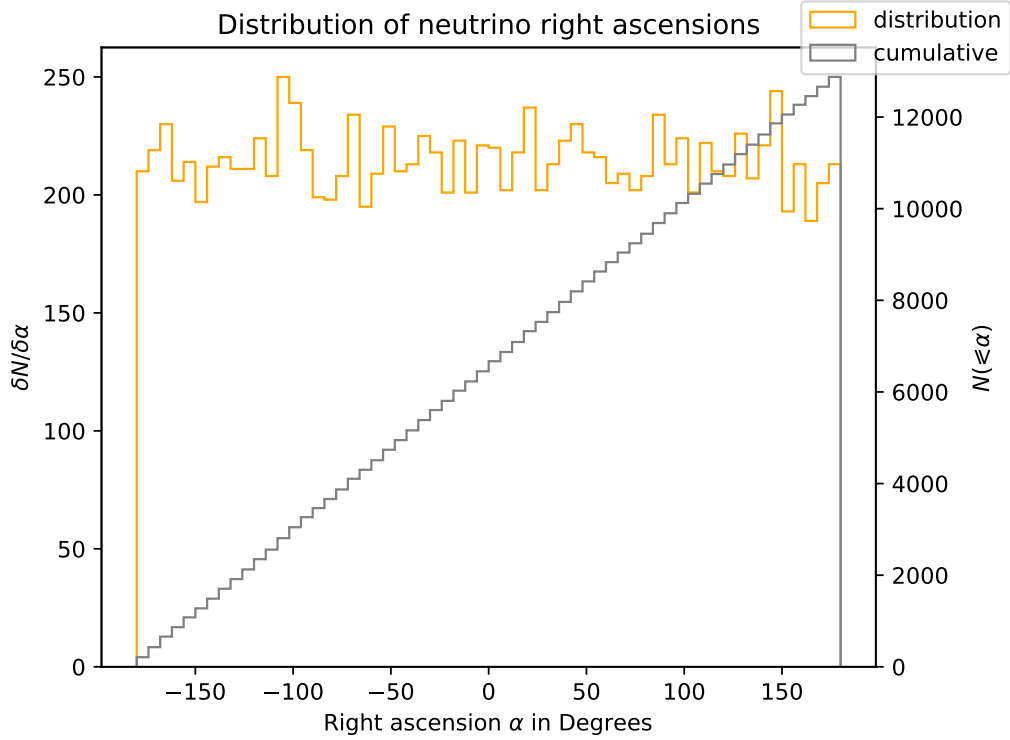


Figure 4.2: The distribution of neutrino right ascension in orange. The cumulative distribution of neutrinos right ascension in gray.

For every realization of a pseudo experiment we match neutrinos to GRB sources and give the time differences in a histogram. We stack all these histograms together to find the background distribution of observed time differences, τ . We can use the same pseudo experiments to find a stacked histogram of the observed time differences over one plus the redshift, τ_z , and of the observed time differences over the distance to a source times the neutrino energy, τ_{LIV} . We will use 500.000 realizations of the background distributions for τ_z and τ_{LIV} to calculate the probability of finding a single match with a certain time difference bin. The probability per bin, k , is given by $p_k = n_k/n_{tot}$, where n_k is the number of matches per bin, and n_{tot} is the total number of matches in a stacked histogram. Using p_k in 4.4, we can calculate the test statistics, ψ , ψ_z , and ψ_{LIV} .

4.3.2 Simulating signal

After having considered the background only case we generate pseudo experiments with a known signal. These new pseudo experiments can be

used to test our data against an alternative hypothesis comparable to the one suggested in section 4.3: “ $n\%$ of all Gamma Ray Bursts have emitted an observed neutrino”. This is done by first scrambling the data using the method described above, and then injecting the signal. We define the signal so that a fraction of randomly selected GRBs will be matched to a random neutrino. We achieve this by changing the neutrinos observation time and position to exactly match that of a GRB. We have repeated this for injected signal fractions of 0.1%, 1%, 3%, 10%, and 30%. We have chosen to replace the neutrinos instead of the GRBs when we simulate signal, since this leaves the background of neutrinos around a GRB unchanged. Another effect of changing the GRB sources instead of the neutrinos would be the possibility of placing a GRB at the edge of the data taking time. As discussed in section 4.2.2, we want to prevent this as it can introduce boundary effects.

We have explained how to inject signal into a realization. Each realization can be used to calculate the time differences and respective test statistics. This gives us a pdf for the null hypothesis, where all neutrinos matching to GRB come from background, but also for some alternatives, where the fractions of signal given above could come from a cosmic source. The next step will be comparing this to the observed data. We can calculate the p-value for every pdf and see how consistent it is with experimental observations. From now on we will denote the fraction of injected signal simply with f .

4.4 Performance

4.4.1 Expectations from background

After deriving the conditions of a match and defining how to generate pseudo experiments it is insightful to consider how many matches we can expect from a pure background distribution. For this we start of with the assumption that both the neutrinos and the GRB are distributed uniformly over the sky and time. We have 12875 neutrinos in the IceCube data collected from April 2008 to May 2009 and 58 GRB that have been observed in the northern hemisphere in the same 400 day period. We have set boundaries on the search cone size in section 4.2.1. The search cone size can vary in size from 1.1° to 3° , as given by equation 4.6. We expect to find between 2.4 neutrinos per GRB if the search cone is 1.1° and 17.7 neutrinos per GRB if the search cone is 3° . If we consider the distribution of GRB positional errors (figure 3.7) we will see that only 5 sources have an error above 1.1° .

Hence most search cones will be of the smaller size. We have defined a match between a neutrino and a GRB if the time difference between their observation is smaller than 40 days we will have to account for this too. For this time window size we expect every GRB to have between 0.46 and 3.45 neutrinos matching to it. This means that for our sample of 58 GRBs we expect 26 neutrinos to match to 26 GRBs if all have a small error of the order of 1° . Or if all GRBs were to have a positional error of the order of 3° we expect 201 neutrinos to match to 58 GRBs. The upper bound of number of matches is estimated way to high due to the small number of GRBs that actually have such a big positional error. Taking into account that only 5 GRB have a big positional error, a more realistic range of 26 \sim 46 neutrinos is expected to match to 26 \sim 31 GRBs. In figure 4.3 an overview for the expected number of coinciding neutrinos per GRB for different search cone and time window sizes is given. This figure is made with the assumption that neutrinos and GRBs follow an isotropic distribution over the sky and a homogeneous distribution in time. It is clear that even if future work reveals that neutrinos can not come from GRBs we still expect some of the events to coincide. This is simply due to the large number of neutrinos that are measured by IceCube. For clarity lines of constant number of coincidences are added to this figure.

We can compare the educated guess above to the simulated background as discussed in 4.1. Before considering the stacked time differences and deriving the pdf of the test statistic, ψ , we will first consider a much simpler counting approach. This means we only count the number of coincidences per pseudo experiment, n_{coinc} and find a pdf of this number. This distribution is derived from generating 500.000 background pseudo experiments and can be seen in figure 4.4. This distribution is used as the pdf of the null hypothesis: "None of the observed neutrinos are produced by Gamma Ray Bursts". The number of coincidences we expect from background is given by $\langle n_{coin} \rangle$, and the number of coincidences that correspond to a 3σ fluctuation above the mean $n_{3\sigma}$ is also shown. As we can see in this figure the peak lies within the expectations from our educated guess. We have also calculated the curves corresponding to the number of coincidences we have found in the actual IC40 data, $n_{coin,data}$. This number will be obtained in section 4.4.3. Before applying the goodness of fit test to this scenario we will compare the data we have used to that in [28]. This is most obvious by considering the stacked time differences of the background distribution. The stacked time differences of the background distribution is shown by the blue lines in figure 4.5.

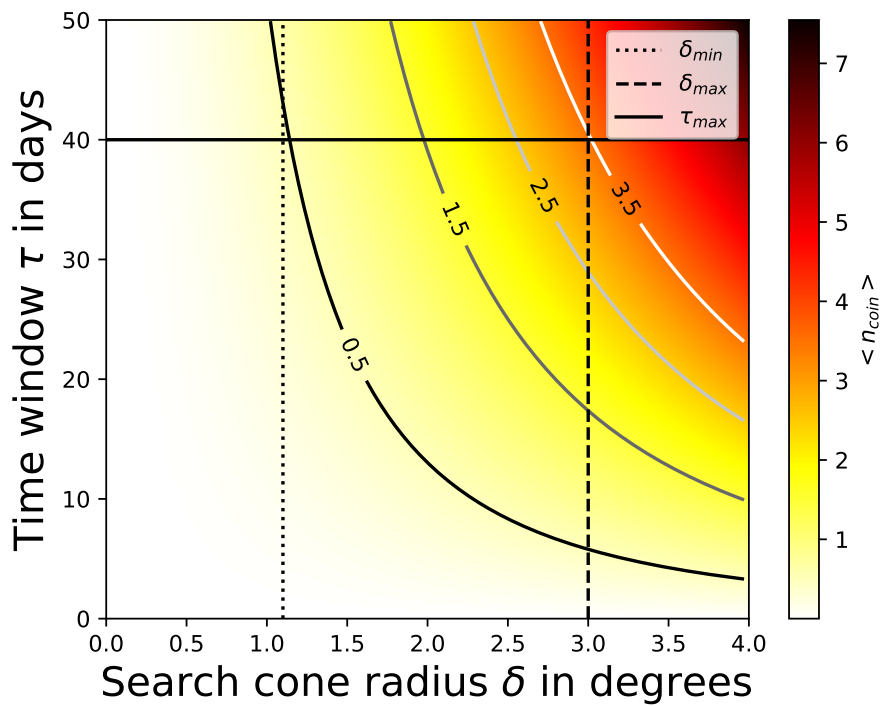


Figure 4.3: The expected number of neutrinos matching per GRB as derived for the IceCube 40 data. The curves corresponds to sets of boundaries that will lead to a given number of matches per GRB.

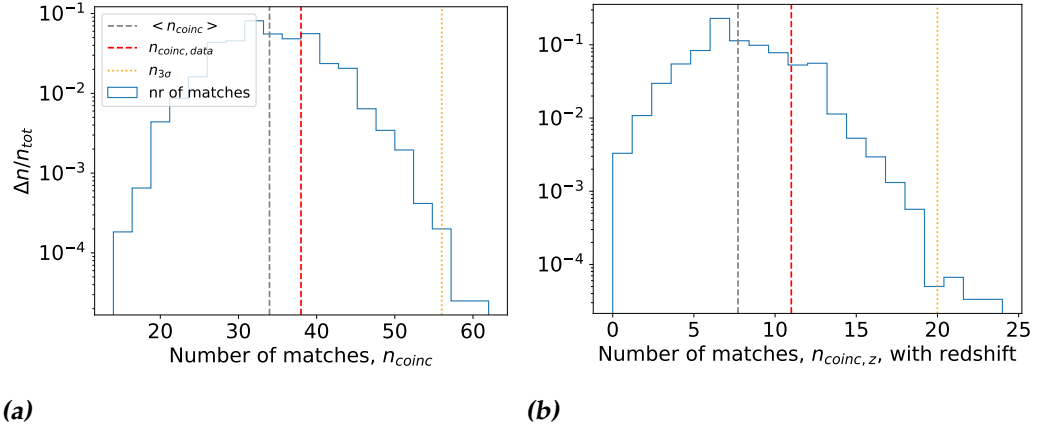


Figure 4.4: The normalized distribution of the number of coincidences, n_{coinc} , for the uniform background of sources without (a) and with (b) redshift. The gray dashed line gives the expected number of coincidences, $\langle N_{\text{coinc}} \rangle$. The red dashed line gives number of coincidences found from the IC40 data, $n_{\text{coinc,data}}$. The orange dotted line gives the number of coincidences for a 3σ fluctuation from the mean.

4.4.2 Sensitivity

Besides the null hypothesis we want to test for an alternative too. For this we have generated pseudo experiments with different fractions of injected signal. These are shown together with the background distribution in figure 4.5. In this figure three different scenarios are probed. The observed time differences, τ are given in figure 4.5a. The intrinsic time difference of the source is probed by the time difference over the redshift, τ_z , given in figure 4.5b. The LIV induced time shift is probed best by τ_{LIV} , in figure 4.5c, the time difference over the distance to a source times the neutrinos energy. For each scenario we have also derived the corresponding test statistic ψ . We have shown together the background distribution and different simulated signals. The pdfs of ψ are plotted in figure 4.6, the blue line again corresponds to the background case and the colors to different injected fractions of signal. Before we compare the results however it is important to note some key differences.

The GRB data that was used previously in [28] could not be exactly reproduced as it was not publicly accessible. The analysis is thus repeated with 58 GRB candidate instead of 60 that were present in [28]. Another difference in the GRB data comes from the information on redshift measurements. Since at present some of the sources have a redshift estimate,

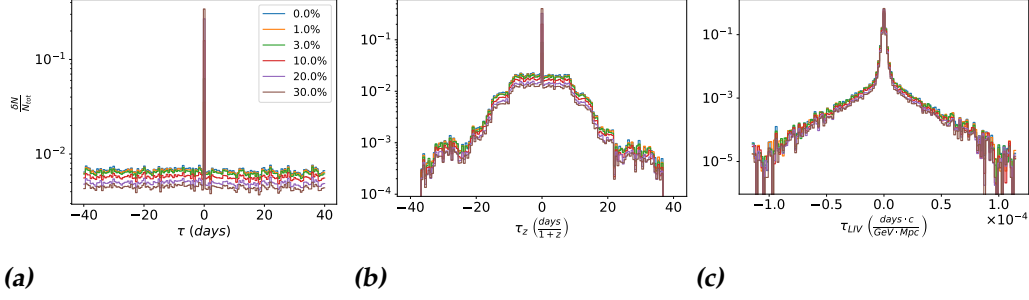


Figure 4.5: The stacked time differences for the three different physics cases and different injected fractions of matching neutrinos in percentage. Note that this plot is normalized and gives the time differences for 500.000 stacked realizations. In plot a we see the time differences, τ , as measured by our telescopes. In plot b we see the time differences at the moment of emission τ_z . The redshift is used to extrapolate the observation times back to the emission times. In plot c we see the Lorentz invariance corrected time difference, τ_{LIV} in units of $\frac{\text{days} \times c}{\text{GeV} \times \text{Mpc}}$.

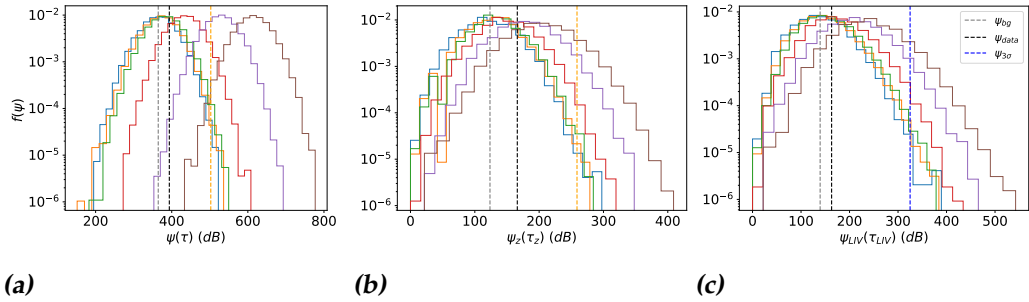


Figure 4.6: The normalized distribution $f(\psi)$ for a different fraction of injected matching neutrinos in percentage. All the three different physics cases are shown above (τ , τ_z , τ_{LIV}). The gray dotted line gives ψ_{bg} the average value of the background distribution. The black dotted line gives ψ_{data} , the value found from the original data. The blue dotted line gives $\psi_{3\sigma}$, the value corresponding to a 3σ fluctuation above background.

f	$1 - P_{bg}$	$1 - P_{3\sigma}$	$1 - P_{z,bg}$	$1 - P_{z,3\sigma}$	$1 - P_{LIV,bg}$	$1 - P_{LIV,3\sigma}$
0%	0.56	0.00126	0.51	0.00030	0.50	0.0006
1%	0.59	0.0011	0.69	0.00040	0.58	0.00014
3%	0.79	0.0028	0.73	0.00060	0.64	0.00090
10%	0.97	0.078	0.84	0.0031	0.80	0.011
20%	1.0	0.83	0.92	0.049	0.92	0.042
30%	1.0	1.0	0.97	0.14	0.98	0.12

Table 4.2: Here we see the results from pseudo experiments with different injected fractions of matching neutrinos, f . $P_{bg,i}$, $P_{3\sigma,i}$ give the probability of finding $\psi_{pseudo,i} \geq \psi_{threshold,i}$, where $i = [z, LIV]$.

that was not known at the of publication from the previous work. We now have redshift information of 17 GRBs instead of only 12. As a result we expect to find one less coinciding GRB neutrino without redshift, but we expect to find almost twice as many coincidences with redshift. Another important difference comes from the way we inject the signal. In [28] signal is injected of the form $5days \times (1 + z)$. It is assumed there that a hypothetical GRB neutrino will be emitted 5 days after a GRB photon. The redshift is included in the signal to account for the effect the traveling distance has on the difference in arrival times in the detector. Looking at other literature that suggested LIV effects, for example in [34, 36], an intrinsic time shift of the order of 10^2 seconds is derived. Since we do not have a good model to decide on an intrinsic time shift we have chosen to inject our signal with an observed time difference of $\tau = 0$. This leads to a difference in the location of the peaks in the histograms. The step-like distribution in figure 4.5b comes from the small number of redshifts we have in our GRB data to sample over.

From the pdf of ψ we can derive the discovery power of the test for a given signal. This is given by the probability that a pseudo experiment gives a test statistic above a threshold value, ψ_c . We integrate the areas of the different curves in figure 4.6 from the threshold value. An overview of the results is given in table 4.2. Here we see the probability of finding a value of the test signal above the given threshold.

4.4.3 Results from IceCube 40

So far we have only used pseudo experiments to see how strong we can make any claim. Now it is time to look at the original data and see how it matches to GRB sources. We have already done an educated guess at how

many neutrinos we can expect from matching them to GRBs in section 4.4.1. Here we show the results of matching IC40 following the scheme described before. The goodness of fit test can be used on the simple counting approach of the background distribution we have given in section 4.4.1. Keeping in mind the differences between our data and that used in [28] we compare our results. In the previous work 42 neutrinos, of which 8 have a known redshift, were found to match to a GRB, while only 35 (4 with redshift) were expected. In our analysis of an almost similar data set we have found 38 coincidences, were only 34 were expected for the total sample. If we consider only GRBs that have a redshift measurement we find 11 coincidences where 7.7 were expected. Going back to figures 4.4 we see that these values lie well within the range of the background pdf.

The probability to find a value like the one of the data or higher, in the background distribution, is 39%, or 0.86σ for sources without redshift. For sources with redshift we find 16%, or 1.41σ , above the expectation from background. In [28] a fluctuation over the expectation from background of only 13.5% (no redshift), and 5.1% (with redshift) was found. The differences in outcome will be due to the lack of 2 GRB sources in our data and the higher number of GRB sources with a redshift measurement. In both our study and that in [28] this first analysis does not lead to rejecting the background scenario.

We have shown that the number of matches correlates well with the background case. It is now insightful to consider how the test statistic compares to the background case. We have to consider three different scenarios for this. We plot the distribution of ψ for a flat background case in blue in figure 4.6. We can use this distribution to see how well the pseudo experiments match the data, which is given by ψ_{data} . As before we will also show the values of ψ at the 3σ significance level. In table 4.3 an overview of the relevant values of ψ for all three physics cases for the background distribution are given. The probabilities, P , to find values above the measured ψ_{data} , and the average number of matches per pseudo experiment, $\langle N_{coinc} \rangle$ are also given in this table. If we compare the values of ψ found from IC40 data to the pseudo experiments which simulate the background we find that 26% of the distribution lies above ψ_{data} . For the sources with a redshift measurement this is even lower. Here the fluctuation above expectation from simulated background is only 13%. These fluctuations correspond to 1.13σ , and 1.51σ respectively.

The stacked time difference histograms of the IceCube 40 data are given in figure 4.7. We have shown the time difference of 38 neutrinos that were associated with 24 GRBs here. This fortifies our believe in having only accidental background matches even more since there is no obvious pre-

	ψ_{data}	P	$\psi_{3\sigma}$	$\langle N_{coinc} \rangle$	N_{data}
τ	394	0.26	503	34.0	38
τ_z	166	0.13	259	7.7	11
τ_{LIV}	163	0.35	324	7.7	11

Table 4.3: The values of the test statistic as derived from the original data ψ_{data} , and at the 3σ limit $\psi_{3\sigma}$. The probability, P , to find a result bigger than ψ_{data} , in the background distribution, the expected number of coincidences, $\langle N_{coinc} \rangle$, and the found number of coincidences N_{data} .

ferred time shift in this histogram. We have also shown the probe of the intrinsic time shift and LIV induced time shift respectively. We see that only a small portion of the matches actually has a redshift measurement and thus a measure of τ_z or τ_{LIV} . We have only found 11 neutrinos matching to 8 GRBs with a measured redshift.

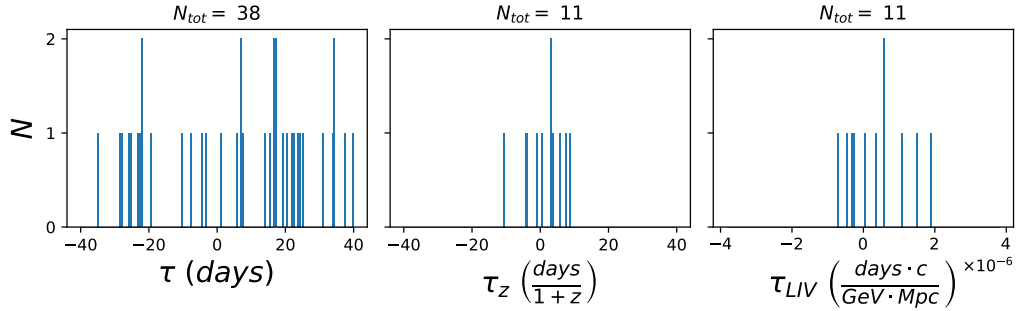


Figure 4.7: The distribution of the stacked time differences between a neutrino and its associated GRB. We have shown all three physics cases side by side. N gives the number of matches in a certain time difference bin, and τ_i gives the time difference of a match.

The last test we can do on this data is comparing it with an alternative hypothesis as formulated in section 4.3.2. We have injected the signal with an observed time difference of $\tau = 0$. This signal is visible in all three physics cases under consideration.

We can guess what will happen to ψ for a higher matching fraction. As long as the injected fraction f is small we expect there not to be a big effect. In fact for the 34 matching neutrinos in the original data set we have calculated $\psi = 394.58$. When we inject a fraction of $f = 0.1\%$ we expect there to be an extra matching neutrino in only a small fraction of the pseudo experiments. A single extra neutrino in the time difference

f	P	P_z	P_{LIV}	N_{GRB}	$N_{z,GRB}$	N_{pairs}	$N_{z,pairs}$
0%	0.26	0.13	0.32	21.69	6.14	33.97	7.72
1%	0.41	0.24	0.42	22.31	6.34	34.94	8.03
3%	0.48	0.23	0.49	22.91	6.51	35.97	8.30
10%	0.86	0.39	0.65	25.28	7.23	40.08	9.49
20%	1.0	0.73	0.83	28.43	8.20	46.16	11.34
30%	1.0	0.85	0.93	30.81	8.93	51.22	12.72

Table 4.4: Here we see some of the results from the pseudo experiments with different injected fractions of matching neutrinos, f . N , N_z give the average number of matches per pseudo experiment for either the GRBs or the total GRB neutrion pairs. P , P_z , and P_{LIV} give the probability of finding $\psi_{pseudo} > \psi_{data}$.

histogram will result in an increase of $\psi \in [3, 12]$, depending on how many matches were already present in the bin it gets added to. As a result we see for the ψ distributions in figures 4.6 that the lower injected fractions are similar to the background data. Only when we go to a higher matching fraction the shift in ψ becomes clear. Table 4.4 gives an overview of the results from 500.000 pseudo experiment with different injected fractions. As expected the portion of a pdf that lies above our data increases as we increase the strength of our simulated signal.

We can conclude that we were not able to distinguish a significant signal over the expected background. This is in agreement with the findings in [28] from analyzing similar data. In a more recent studies [34, 36] the association of high energy neutrinos to GRB sources has been used to derive a value of the intrinsic time shift at the source and the LIV energy scale. Even though we have shown that our data does not show a significant excess of signal we will still see what size of LIV shift we can derive from this. We do this with the assumption that all neutrinos matched to a source with redshift are GRB neutrinos, which is obviously not justified.

To find a value for the LIV scale we have to use equation 4.2. We can go about this in two ways. We assume a LIV effect at $E_{LIV} = 6.4 \times 10^{17}$ GeV, and $\Delta t_{in} = 280$ seconds as given in [34]. Then we use equation 4.2 for each matching pair. The time difference that we find is the expected time difference in days, $t_{expected}$, if $E_{LIV} = 6.4 \times 10^{17}$ GeV, and $\Delta t_{in} = 280$ seconds. This shows a big disagreement with the observed time difference suggesting once again that our data does not show a LIV shifted signal, but rather a background signal.

We can also follow another approach, and derive the size of LIV scale and intrinsic time shift that we would find if the matches we have found

GRB	z	E_ν	t_{obs}	$t_{expected}$
080810A	3.35	2.00	3.85	0.06
081228A	3.8	1.71	3.25	0.06
081228A	3.8	2.75	-4.54	-0.08
080707A	1.23	1.67	8.67	0.02
080707A	1.23	3.03	3.15	0.04
080604A	1.416	11.28	-10.60	-0.14
080604A	1.416	1.76	-1.32	-0.02
080607A	3.036	1.30	0.30	0.04
080603B	2.69	1.20	6.09	0.03
090102A	1.547	1.88	-3.91	-0.02
090323A	3.57	1.98	7.38	0.06

Table 4.5: The candidates of IC40 neutrinos that are associated with GRBs. Time differences are given in days / $(1 + z)$, and the energy in TeV.

are all GRB neutrinos. As in [34, 36] we interpret equation 4.2 as a linear equation of two variables. For every matching pair we can use the observed time shift, redshift, distance to a source, and the neutrinos energy as parameters in two variables, $x = \pm E_\nu \cdot \frac{D(z)}{c}$, and $y = \frac{\Delta t_{obs}}{1+z}$. We can interpret the unknown constants as, $A = \Delta t_{in}$, and $B = \frac{1}{E_{LIV}}$, which are the values we want to find.

$$\frac{\Delta t_{obs}}{1+z} = \pm \frac{E_\nu}{E_{LIV}} \frac{D(z)}{c} + \Delta t_{in}, \quad (4.8)$$

$$y = A + B \cdot x$$

To do the actual fitting we follow the least-squares fitting approximation as it is explained in [77, 78]. This allows us to find A , and B , and hence the LIV scale and intrinsic time difference. In figure 4.8 we have plotted the associated neutrino GRBs in blue and fitted a line to this with the approach explained above. The slope of the line corresponds to 1 over the LIV energy scale, $E_{LIV,fit} = (8.2 \pm 0.045) \cdot 10^{15}$ GeV, and the zero crossing point corresponds to the intrinsic time shift, $t_{in,fit} = (9.5 \pm 7.6) \times 10^4$ seconds. More detail on the least-squares fit can be found in appendix B.

Our results corresponds really well with a linear relation. This is partly due to our freedom of choice in sign for the LIV factor. By using a $-$ sign for the LIV scale of delayed events and a $+$ sign for the LIV scale of advanced events we have introduced a linear correlation to the results. We will leave quantifying this artificial effect for a future study and try to give a measure of how well our result corresponds with a linear relation. This is

done in terms of a correlation coefficient following the approach of [34, 36]. For our data we find $r_0 = 0.87$. To know what this tells us we can calculate the probability to find a correlation coefficient bigger than this value from the same amount of uncorrelated events. This is $P(|r| > |r_0|) = 0.16\%$. The formulas to calculate the correlation coefficient and the probability to find this value are given in appendix B.1. This does not agree with [34], where a LIV scale of $E_{LIV} = (6.5 \pm) \cdot 10^{17}$ GeV and an intrinsic time shift of $\Delta t_{in} = (1.7 \pm 3.6) \cdot 10^3$ s was found for a correlation coefficient of $r_0 = 0.98$. In [36] the LIV scale is found at $E_{LIV} = (6.4 \pm 1.5) \cdot 10^{17}$ GeV, and the intrinsic time shift at $\Delta t_{in} = (-2.8 \pm 0.7) \cdot 10^2$ s, at a correlation coefficient of $r = 0.989$. This again does not match our results. The main difference in the IC40 data and that used in the studies showing LIV effects is that neutrinos that were matched to source with a similar time difference between neutrino and photon arrival times have a much higher energy than in the IC40 data. Neutrinos of similar energies however were in [34, 36] found to match to a source with a much smaller time difference.

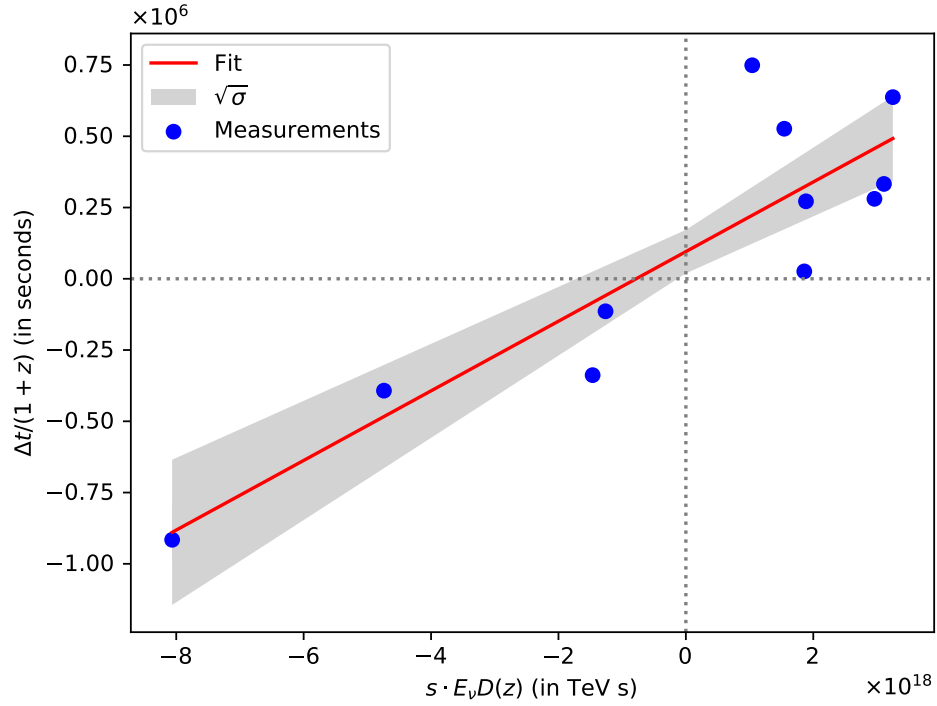


Figure 4.8: A linear fit to the observed time difference over redshift and neutrino energy times distance to the source. s is the LIV sign factor which is negative for delayed neutrinos and positive for advanced neutrinos. The gray region is given by the variance of our fit, σ . The observed time differences are given in blue.

IC79 and IC86

In November 2016 the IceCube collaboration has published new neutrino data [63]. We will use the analysis developed in the previous chapters on this new data set. The data is collected from June 2010 to May 2013, when the IceCube detector was still being completed. During this time it had 79, and 86 strings actively detecting neutrino events going both up and down in the detector. We combine this with data from GRBweb from the same period and apply similar selection criteria as was done for IC40 data. We can however not treat the newer data exactly the same as the IC40 data. First we note that the IC40 data only consisted of up-going neutrinos, while the newer data shows both up- and down- going neutrino events. This means we have to consider GRBs in both parts of the sky. Another difference comes from the fact that the detector was still being constructed during this new data taking period. During its construction the event selection criteria were also changed [63]. This means we have to be more careful about selecting data.

The most obvious change in the detector during the collection of IC79 and IC86 data comes from adding 7 strings more to the detector, increasing its detection volume. In the section 5.1 we will look into this in more detail. For now we only consider the neutrino data at hand. Even during the 2 years in the 86 string configuration the number of events in the data is not constant over time. We have shown the number of detected neutrino events as a function of the detection time in figure 5.1a. In this figure a jump in the number of events can be seen on the boundaries of the different data taking periods. Since these jumps come from the detector configuration and data selection by the IceCube collaboration [63], we do not want to include them in our analysis. We want the result of our analysis to be as independent as possible from data taking conditions.

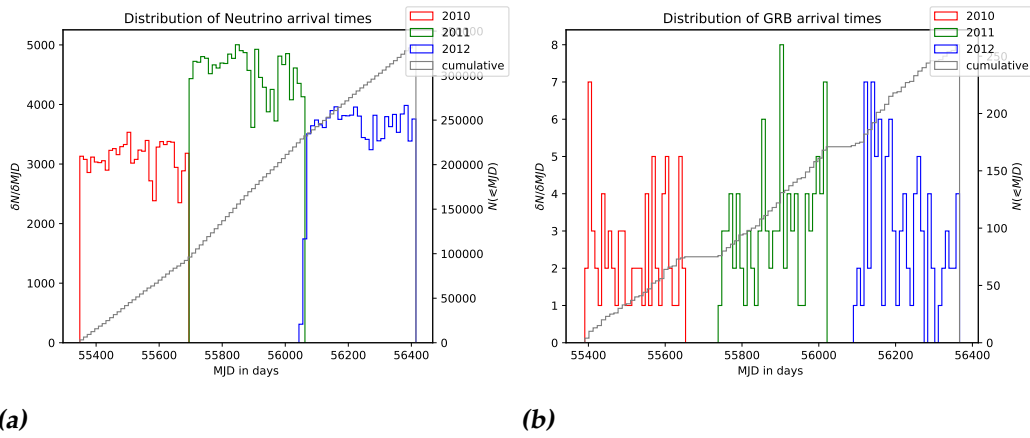


Figure 5.1: The distribution of neutrino MJD in the data collected from June 2010 to May 2013 in 5.1a. There are big changes in number of events between the different data taking periods. The GRB MJD distribution given in the right panel. The gaps in the GRB data come from the selection criterion that no GRB lies in the boundary region.

We eradicate boundary effects due to the change of data collection by excluding all the GRB sources that fall within the boundary regions of data taking. If we are to explore a 40 day time window for example, we want to exclude all GRBs that have occurred within 40 days from the edges of neutrino data taking. Figure 5.1b illustrates the selected GRB sources in the full sky, after removing all bursts within 40 days of the data taking periods. The equatorial positions of each selected burst can be seen in figure 5.2. The color is used to denote the time of observation. The first selection based on the observed time of has already reduced our GRB sample by a lot. From the 5334 bursts that we have in the GRBweb catalog only 260 are left.

5.1 Effective area

As we have explained the IceCube detector has been detecting events, while it was being constructed further. One of the ways of quantifying the change in the detector efficiency, is considering the effective area of the detector. The effective area gives us a measure of how efficient a detector can detect events and depends on the event energy and incident direction. This area is defined as the ratio between the detected neutrino event rate and the incoming cosmic neutrino flux. The IceCube collaboration has published data on the effective area of the detector [63]. We can

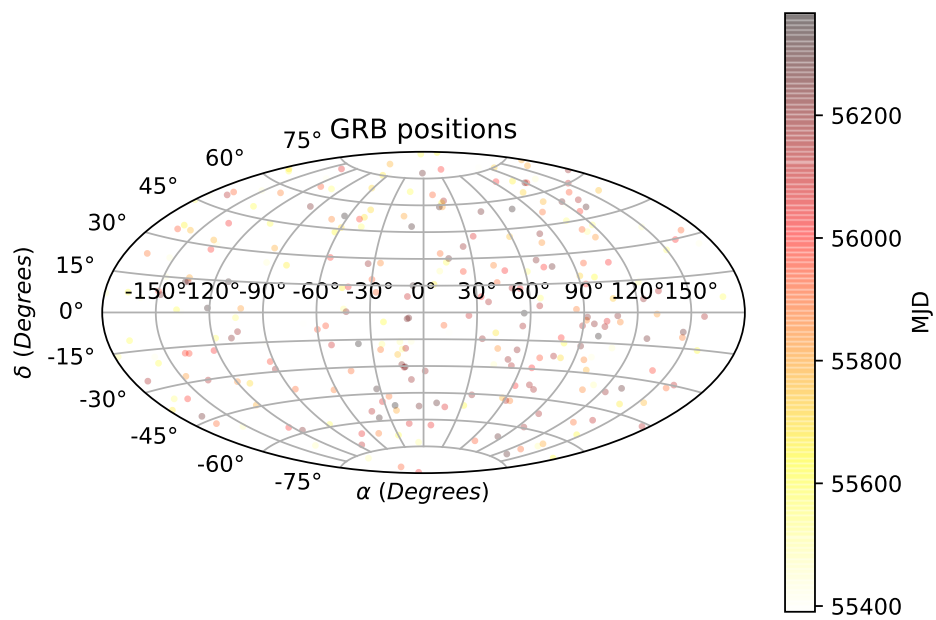


Figure 5.2: The distribution of GRB positions and observation times.

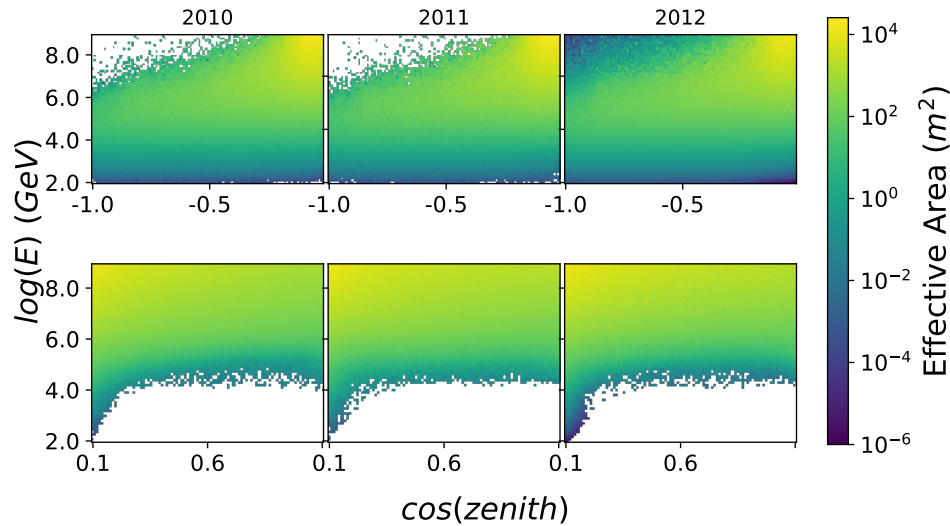


Figure 5.3: The effective area of the IceCube detector during three different time periods as a function of neutrino energy and incident zenith angle. The effective area for neutrinos that come from the northern hemisphere are shown in the upper three panels. The effective area for neutrinos coming from the southern hemisphere are given in the lower panels

look at the different periods and see that the effective area has changed over time. We show the effective area as a function of energy and incident zenith angle in figure 5.3. The effective areas for both up-going neutrinos, which come from the northern hemisphere, and down-going neutrinos, which come from the southern hemisphere are shown separately. In figure 5.4 we have shown the number of neutrinos detected per declination bin. This shows a strong dependence of the number of detected events and the declination of the impinging neutrino. Both 5.3, and 5.4 are split up in a northern and southern hemisphere part. In section 5.2 we will argue why this split is chosen. We can also see different energy selection criteria in figure 5.4, denoted as $E_f = x\%$. This selection will also be explained in the next section.

5.2 Energy selection

Figure 5.3 shows the effective area of the IceCube detector for both the northern and southern hemisphere. From this figure we see that the ef-

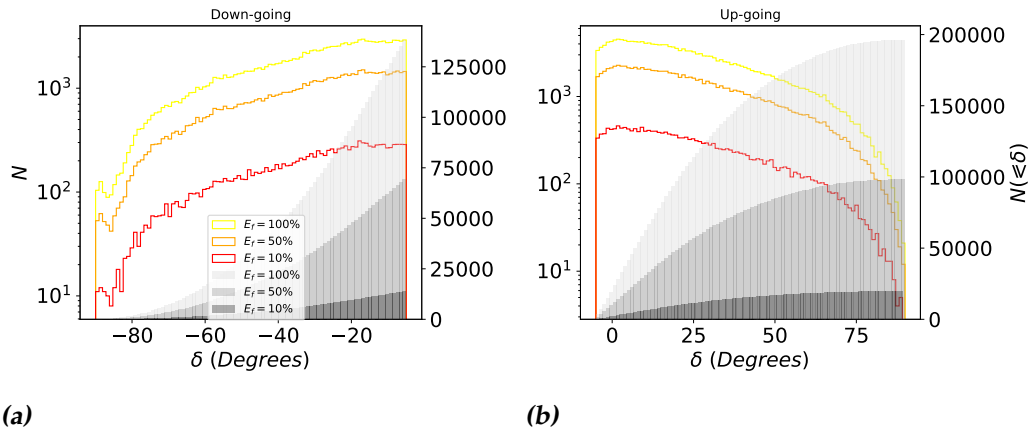


Figure 5.4: The distribution of neutrino declination for both the up- and down-going neutrinos. The different energy selection criteria are also shown.

fective area depends strongly on both the events energy and the incident declination. If we consider the data that is provided by the IceCube collaboration [63] we see that the neutrino energies vary greatly depending on their declination. Up -going neutrinos have traveled through the Earth. We have discussed in chapter 3.1 that the Earth will remove a big portion of the atmospheric muon signal that is detected by IceCube. Unfortunately it also works as a filter for the highest energy neutrinos which are most likely to show a noticeable LIV effect. Figure 5.5 shows the relation of neutrino energy and incident declination for all three years of data taking. In this figure we have also shown where we will split up the sky. This split is chosen at -5° declination following the choice of the IceCube collaboration [63]. They argue that this is the angle from which absorption of high energy neutrinos by the Earth becomes an important factor. The effect of this absorption can be seen by the lack of high energy events for positive declination.

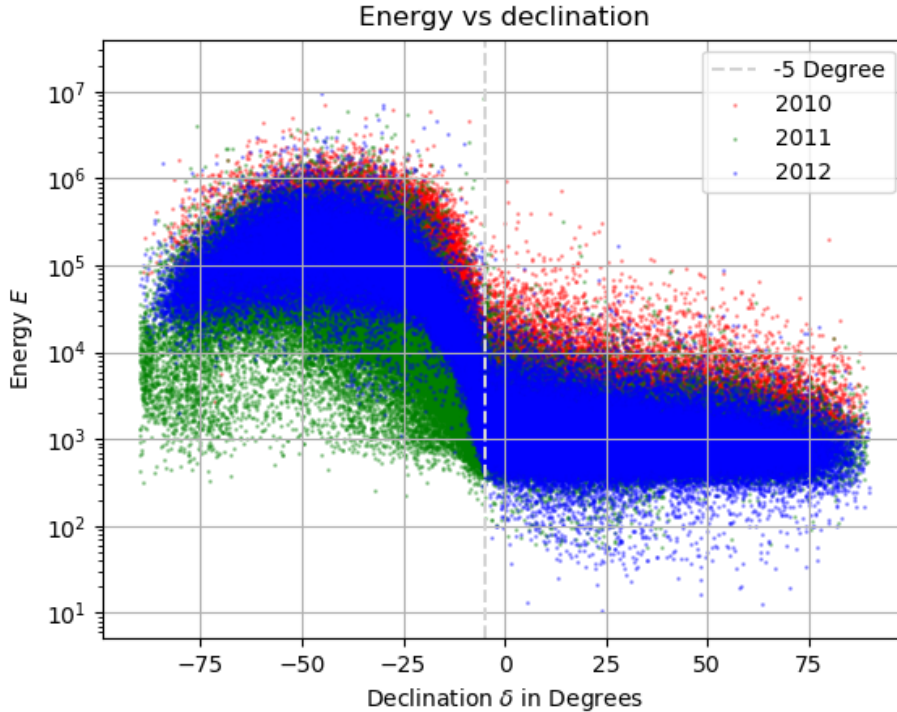


Figure 5.5: The distribution neutrino energies per year (color coded) as a function of declination. The lightgray line denotes where we split the data.

When we compare the distribution of the neutrino energies in the two parts of the sky, we see that the spectrum is different. In the northern hemisphere we expect to observe less high energy neutrinos than in the southern hemisphere due to the filtering by the Earth. In the southern hemisphere however, a large amount of the detected events is likely to stem from atmospheric muons. The yellow lines in figure 5.6 show the distributions of neutrino energies in the both southern and northern hemisphere respectively. The other lines correspond to a selection based on the neutrino energy explained below.

After applying the declination split on the neutrino data, we have 138.361 neutrinos in the southern hemisphere, and 196.314 neutrinos in the northern hemisphere. We can match them to 139 GRBs in the southern hemisphere and 121 GRBs in the northern hemisphere. As in section 4.4.1 we can calculate how many neutrino to GRB associations we expect to find if the data is uncorrelated. We assume that the number of neutrinos we measured is randomly distributed over the sky, and consider how many neutrinos we would expect to coincide with a GRB. This gives us an es-

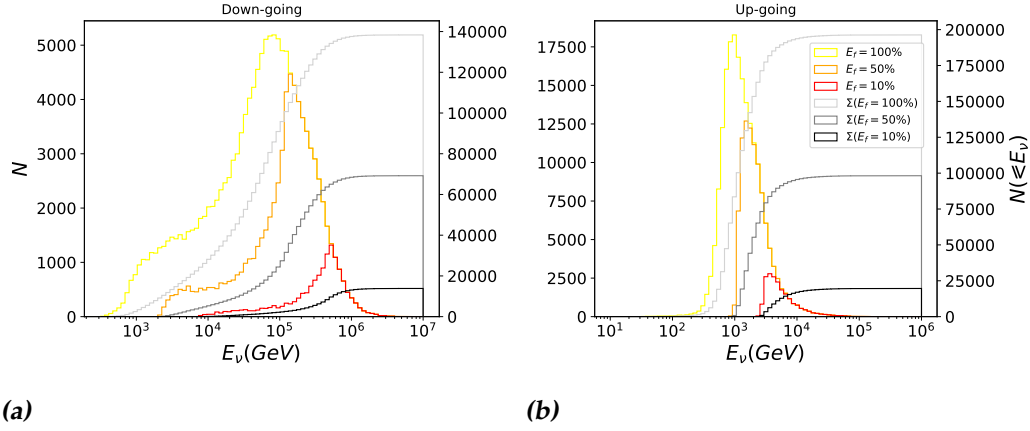


Figure 5.6: The distribution of down-going neutrinos in the southern hemisphere, and up-going neutrino energies in the northern hemisphere after applying different energy selection criteria. The criteria are denoted as a fraction of the total energy denoted by E_f . The gray lines give the cumulative distribution of neutrino energies per selected fraction.

timate of a neutrino background distribution. To calculate the expected number of background neutrinos per GRB we use equation 5.1. We can do our analysis with different search cone boundaries, as discussed in section 4.2. We have plotted the expected number of background coincidences per GRB in figure 5.7 as a function of the time window size, and the search cone radius.

$$\frac{\langle n_\nu \rangle}{n_{GRB}} = \frac{N_\nu \cdot \pi \delta_{cone}^2 \cdot T_{data}}{360^2 \cdot 2\Delta t} \quad (5.1)$$

Here $\frac{\langle n_\nu \rangle}{n_{GRB}}$ is the number of expected neutrinos per GRB source. N_ν is the total number of neutrinos in the data. δ_{cone} is the search cone radius in degrees, similar to δ_{cut} in section 4.2.1. The total data taking time is given by T_{data} and Δt is the search time window, similar to the one derived in section 4.2.2.

We see from the expected number of coincidences in figure 5.7 that we can expect a lot of coincidences from purely background neutrinos. To increase the ratio of signal to background we can apply a cut on the energy. We expect the cosmic neutrinos coming from a GRB source to have relatively high energies, compared to atmospheric neutrinos. Removing lower energy events will thus increase our signal to background ratio. We have to take into account however that the detectors effective area also depends on the neutrino energy, and its incident direction. This means that we can-

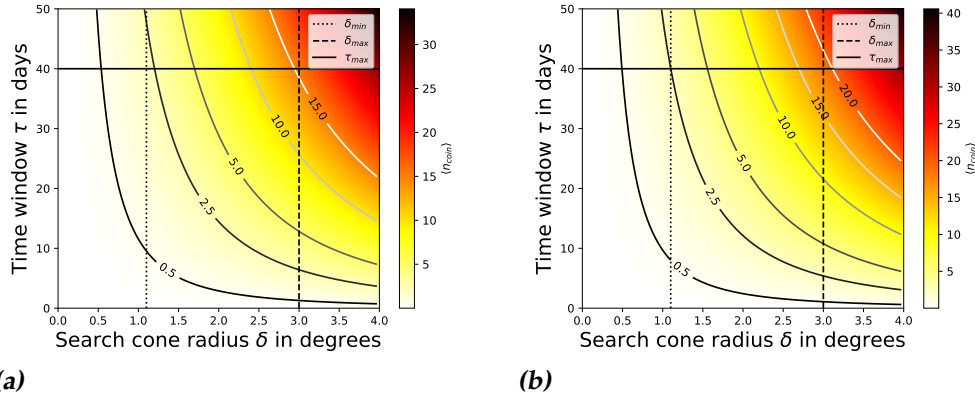


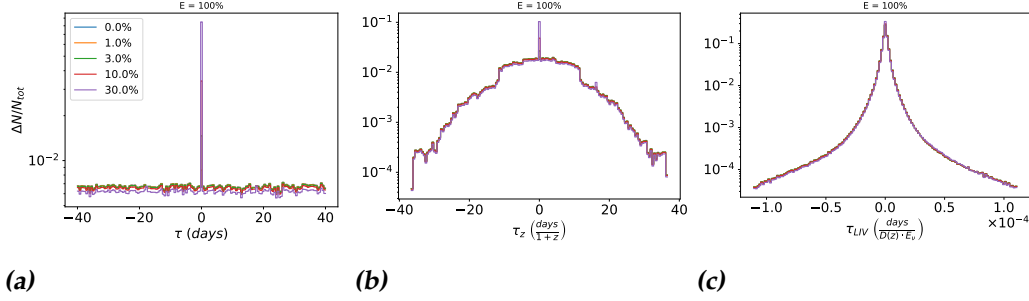
Figure 5.7: The expected number of neutrino matches per GRB in the southern 5.7a, and northern hemisphere 5.7b. Lines of constant number of matches are added in for clarity.

not just remove the $x\%$ lowest energy neutrinos. As this would result in heavily biasing our data for neutrinos impinging from the lowest declination. Figure 5.5 illustrates the energy declination dependence. For the northern hemisphere, we have already seen in figure 5.6a that the energy distribution is relatively flat. For the southern hemisphere however there is a strong relation between the neutrino energies and their declination. An energy cut can be done on a declination dependent basis. Meaning that we take declination bins of 1° size and only include the highest $x\%$ of neutrinos per declination bin. The resulting energy distribution for the highest 50%, and 10% energy neutrinos is in figure 5.6 by the orange and red curves. The cumulative distributions for each energy fraction are also shown in this figure.

5.3 Sensitivity for IC79 and IC86

Before we apply the goodness of fit test to the new data we will first blind it. This means that we have randomized the neutrino detection times, within the period of observation, and right ascensions. This is done to ensure that we will follow an unbiased approach to setting the matching and selection criteria. For the null hypothesis we will again use: 'None of the observed neutrinos are produced by Gamma Ray Bursts.' We test to this hypothesis with the method explained in chapter 4. This means that we can first find a discovery potential of different hypothetical signals and only after having found this we will consider the real data. In figure 5.8

Stacked time differences of Up-going Neutrinos

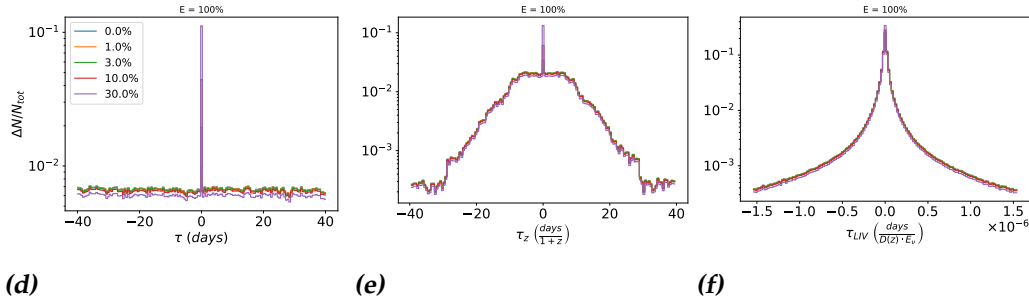


(a)

(b)

(c)

Stacked time differences of Down-going Neutrinos



(d)

(e)

(f)

Figure 5.8: The normalized stacked time differences of 500.000 realizations for the three different physics cases and different injected fractions of matching neutrinos in percentage. In plot a and d we see the time differences, τ , as observed. In plot b and e we see the time difference probe of the emission times τ_z . The redshift is used to extrapolate the observed time difference back to the emission time difference. In plot c and f we see the Lorentz invariance corrected time difference, τ_{LIV} in units of $\frac{\text{days} \cdot c}{\text{GeV} \cdot \text{Mpc}}$.

we see the stacked time differences from associating neutrinos to GRBs. We have considered three physical scenarios to probe, as in section 4.4.2. Again τ corresponds to the observed time difference, τ_z to the time difference corrected for redshift, and τ_{LIV} for the time difference tuned to probe LIV effects. We have included different amounts of injected signal generated according to the strategy described in section 4.3.2. The up- and down-going particles are shown in separate histograms, because we have been separately looking for matches in the northern and southern hemisphere. In appendix C we show results for the same analysis, but this time with a constant search cone of $\delta = 3^\circ$. This is done as an extra control to see how our varying search cone will effect the strategy.

Figure 5.9 shows the test statistic for the same three scenarios of up-

Threshold values of ψ for Up-going neutrinos

Selection		ψ_{bg}	ψ_{data}	$\psi_{3\sigma}$	$\langle N_{coinc} \rangle$	N_{data}
$E_f = 1$	τ	1263	1226	1405	490	462
	τ_z	576	567	718	123	125
	τ_{LIV}	230	224	365	123	125
$E_f = 0.5$	τ	993	987	1117	233	232
	τ_z	412	432	556	60	69
	τ_{LIV}	137	130	237	60	69
$E_f = 0.1$	τ	430	447	571	44	48
	τ_z	146	127	272	12	10
	τ_{LIV}	49	52	116	12	10

Table 5.1: The values of the test statistic as derived from the up-going neutrinos in the original data ψ_{data} , and at the 3σ limit $\psi_{3\sigma}$. The ψ value for the simulated background and the expected number of coincidences, $\langle N_{coinc} \rangle$, and the found number of coincidences N_{data} . Note that the results are given for the three different energy selections.

going neutrinos. We have here also included the results of choosing different energy fractions, E_f . This allows for considering the effect it has on improving the signal to background ratio. Figure 5.10 shows the same test statistics but then for neutrinos traveling down into the detector. Both figures also contain vertical lines to denote the different threshold values, $\psi_{3\sigma}$ and ψ_{bg} . A line for ψ_{data} has been included in figures and tables. This will not be considered until we look at the unblinded data in section 5.4. Tables 5.1 and 5.3 give the numerical values of the threshold values for both the up-going neutrinos and down-going neutrinos respectively. We will use these values to test our find how well we can distinguish different simulated signal distributions from the background. An overview of the sensitivities is given in tables 5.2 and 5.4 for both parts of the neutrino data, and all the different energy selection criteria.

Distribution of the Test statistic for Up-going Neutrinos

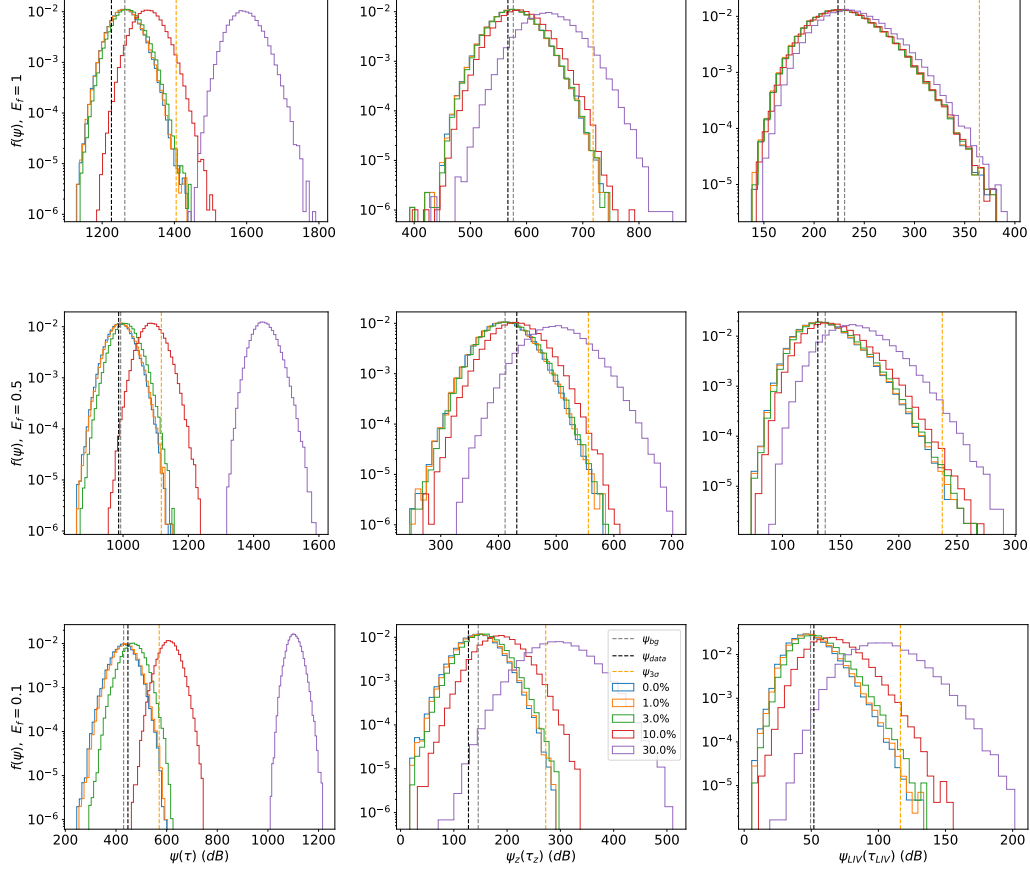


Figure 5.9: From left to right we have shown the normalized distributions of ψ , ψ_z , and ψ_{LIV} for different fractions of simulated signal. The upper row gives the results if we include all neutrinos, the middle row gives the result if we include only the highest 50% energy neutrinos, and the bottom row gives the result for the highest 10% energy neutrinos. The dashed lines correspond to the threshold value. The mean from background, ψ_{bg} , is given in gray, the 3σ value is given in orange, and the black dashed line gives the value of, ψ_{data} we found in our data. An overview of the threshold values can be seen in tables 5.1 and the probability of finding values above this threshold is given in table 5.2. Note that the figures give up-going neutrinos only.

Probability of finding $\psi_{pseudo} > \psi_{bg}$ for Up-going Neutrinos

Selection	f	$1 - P_{bg}$	$1 - P_{3\sigma}$	$1 - P_{z,bg}$	$1 - P_{z,3\sigma}$	$1 - P_{LIV,bg}$	$1 - P_{LIV,3\sigma}$
$E_f = 100\%$	0%	0.50	0.00017	0.50	0.00015	0.47	0.00015
	1%	0.50	0.00015	0.50	0.00015	0.47	0.00016
	3%	0.58	0.00036	0.51	0.00015	0.48	0.00018
	10%	0.97	0.031	0.62	0.00046	0.59	0.00017
	30%	1.0	1.0	0.94	0.035	0.59	0.00035
$E_f = 50\%$	0%	0.50	0.00015	0.50	0.00016	0.46	0.00013
	1%	0.51	0.00020	0.50	0.00018	0.47	0.00016
	3%	0.66	0.0090	0.53	0.00020	0.50	0.00019
	10%	1.0	0.20	0.69	0.0010	0.61	0.00046
	30%	1.0	1.0	0.98	0.12	0.88	0.0046
$E_f = 10\%$	0%	0.50	0.00014	0.50	0.00014	0.47	0.00013
	1%	0.56	0.00026	0.52	0.00021	0.50	0.00016
	3%	0.83	0.0033	0.61	0.00044	0.60	0.00043
	10%	1.0	0.87	0.87	0.011	0.86	0.0044
	30%	1.0	1.0	1.0	0.685	1.0	0.26

Table 5.2: This table gives the probability to find a value of the test statistic above the median from background, P_{bg} , for up-going neutrinos, and above the 3σ value from background, denoted by $P_{3\sigma}$. The probabilities are calculated for different injected fractions of signal, f , and for different energy selection criteria, E_f .

Distribution of the Test for Down-going Neutrinos

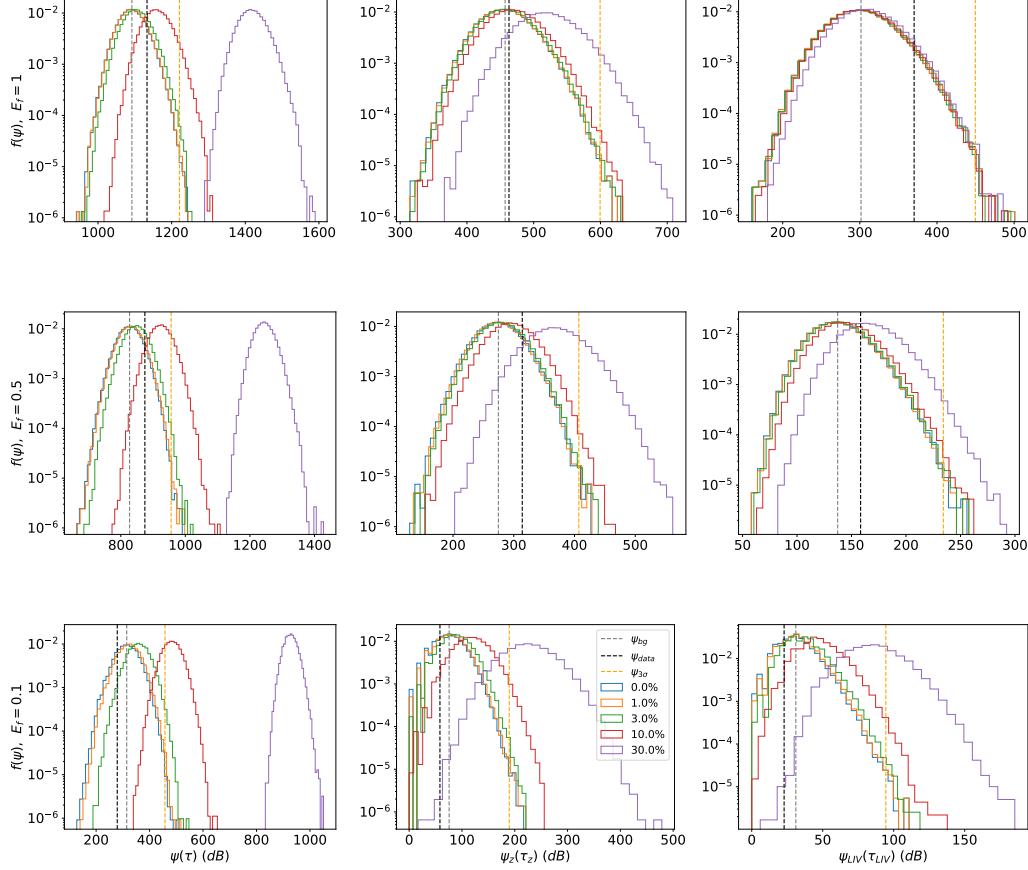


Figure 5.10: From left to right we have shown the normalized distributions of ψ , ψ_z , and ψ_{LIV} for different fractions of simulated signal. The upper row gives the results if we include all neutrinos, the middle row gives the result if we include only the highest 50% energy neutrinos, and the bottom row gives the result for the highest 10% energy neutrinos. The dashed lines correspond to different threshold values. The mean from background, ψ_{bg} , is given in gray, the 3σ value is given in orange, and the black dashed line gives the value of, ψ_{data} we found in our data. An overview of the threshold values can be seen in tables 5.3 and the probability of finding values above this threshold is given in table 5.4. Note that the figures give down-going neutrinos only.

Threshold values of ψ for Down-going neutrinos

Selection		ψ_{bg}	ψ_{data}	$\psi_{3\sigma}$	$\langle N_{coinc} \rangle$	N_{data}
$E_f = 1.0$	τ	1092	1133	1221	304	352
	τ_z	457	463	599	85	103
	τ_{LIV}	301	370	450	86	103
$E_f = 0.5$	τ	827	848	956	149	171
	τ_z	275	314	407	33	45
	τ_{LIV}	137	158	234	33	45
$E_f = 0.1$	τ	315	279	458	27	23
	τ_z	76	58	190	5.3	4
	τ_{LIV}	31	23	94	5.3	4

Table 5.3: The values of the test statistic as derived from the down-going neutrinos in the original data ψ_{data} , and at the 3σ limit $\psi_{3\sigma}$. The probability, P , to find a result bigger than ψ_{data} , in the background distribution, the expected number of coincidences, $\langle N_{coinc} \rangle$, and the found number of coincidences N_{data} .

From figures 5.9 and 5.10, we see that applying the energy selection to reduce the total number of neutrinos in our sample also influences the distribution of the test statistic. Comparing the figures to the associated tables 5.2 and 5.4 we can say something about how the energy selection can improve our ability to distinguish signal from background. Removing more low energy neutrinos will lead to a higher sensitivity to simulated signal. If for example, we want to look for an evidence of a signal associated with 10% of the GRBs. In section 4.1.1 we have defined the significance of our test. We stated that we find a hint for rejecting the null hypothesis, if we find a p-value p_{data} , smaller than $p_{3\sigma}$ as derived from the background distribution. Comparing with the background however is not enough. We also want to know how confident we are in our statement that this value of ψ comes from a neutrino signal of said strength. This is where the pseudo experiments come in. We have simulated a pdf for ψ containing a simulated signal of 10%. If we integrate the surface under this curve from $\psi_{3\sigma}$, as derived from background, to infinity we find the discovery power. Or, in other words, the probability that a value of ψ above 3σ can be associated with this simulated pdf. If this probability is high enough we can state that we have found an evidence for a signal associated with 10% of the GRBs at the calculated discovery power.

In table 5.4 we see that as we select less low energy particles the discovery power increases. Including all particles and looking for a 10% fluctuation over 3σ from background, leads to a discovery power of 4.3% which

Probability of finding $\psi_{pseudo} > \psi_{bg}$ for Down-going Neutrinos

Selection	f	$1 - P_{bg}$	$1 - P_{3\sigma}$	$1 - P_{z,bg}$	$1 - P_{z,3\sigma}$	$1 - P_{LIV,bg}$	$1 - P_{LIV,3\sigma}$
$E_f = 100\%$	0%	0.50	0.00017	0.49	0.00015	0.48	0.00013
	1%	0.51	0.00019	0.50	0.00017	0.49	0.00013
	3%	0.63	0.00061	0.52	0.00018	0.52	0.00020
	10%	0.98	0.043	0.63	0.00048	0.62	0.00038
	30%	1.0	1.0	0.94	0.031	0.90	0.00052
$E_f = 50\%$	0%	0.50	0.00016	0.50	0.00016	0.48	0.00015
	1%	0.53	0.00019	0.51	0.00016	0.49	0.00016
	3%	0.72	0.010	0.56	0.00024	0.52	0.00020
	10%	1.0	0.17	0.74	0.011	0.62	0.00038
	30%	1.0	1.0	0.99	0.18	0.90	0.0053
$E_f = 10\%$	0%	0.51	0.00013	0.50	0.00012	0.48	0.00012
	1%	0.58	0.00026	0.53	0.00013	0.52	0.00015
	3%	0.87	0.0047	0.67	0.00034	0.65	0.00026
	10%	1.0	0.78	0.92	0.015	0.90	0.0022
	30%	1.0	1.0	1.0	0.	1.0	0.31

Table 5.4: This table gives the probability to find a value of the test statistic, ψ_{pseudo} above the median from background, P_{bg} , for down-going neutrinos, and above the 3σ value from background, denoted by $P_{3\sigma}$. The probabilities are calculated for different injected fractions of signal, f , and for different energy selection criteria, E_f .

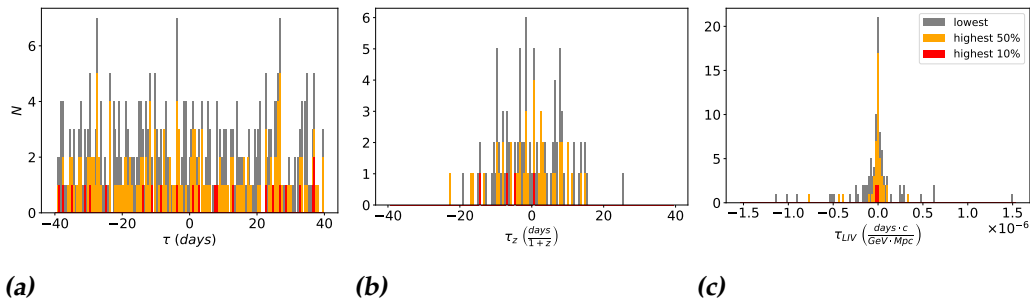
tells us we cannot distinguish the signal from background. If we repeat this analysis for the highest 50% energy neutrinos we find that our discovery power has increased to 17%. This is still too low to say we have found a signal. In the scenario for only the highest 10% energy neutrinos, the confidence level is even higher at 78%. Still to state that we will be able to distinguish this signal from background this will not be enough. We did however learn that, if we want to have the strongest test to recognize any signal at all, we are best off in considering only the higher energy neutrinos.

5.4 Results

We have shown the result of correlating neutrinos to GRB sources for all different energy selection criteria. In figure 5.11 the gray bars denote the total neutrino sample, orange and red bars denote the highest 50% and 10% energy neutrinos respectively. We have again considered the three physics cases for both up- and down-going neutrinos separately. The values of ψ calculated from the unblinded results shown in the figures here was already given in tables 5.1 and 5.3. There we can see that in all cases $\psi_{data} < \psi_{3\sigma}$. We have not found any evidence for a neutrino signal associated with GRB above background. We can still calculate how well our found ψ_{data} compares to the different injected fractions to give a numerical assessment of our statement that no significant signal was found. This way we can at least reject the presence of signal above a certain fraction. In the previous section we have shown that we are most likely to be able to distinguish a signal for only the highest energy neutrinos. Hence, table 5.5 only considers the highest energy scenario. We can also see in figures 5.9 and 5.10 that the spacing between pdfs for different injected fractions increases as the energy selection becomes more constrained. This translates to finding a higher discovery power, as can be seen in the tables 5.2 and 5.4.

From the bottom row in figures 5.9 and 5.10, and table 5.5, we see that the value of ψ_{data} is always smaller than $\psi_{3\sigma,bg}$. This tells us that our signal cannot be distinguished from the background distribution. We can also use the found value ψ_{data} to see if we can reject a signal associated with a certain amount of GRBs. For the observed time difference of the up-going neutrinos we find that, we can reject a signal associated to more than 3% of the GRBs with a confidence level of 70%. We can reject a signal associated to more than 3% of the GRBs at 80% confidence for the observed time difference over $1+z$. For the LIV probed time difference, we can

Stacked time differences for Down-going Neutrinos



Stacked time differences for Up-going Neutrinos

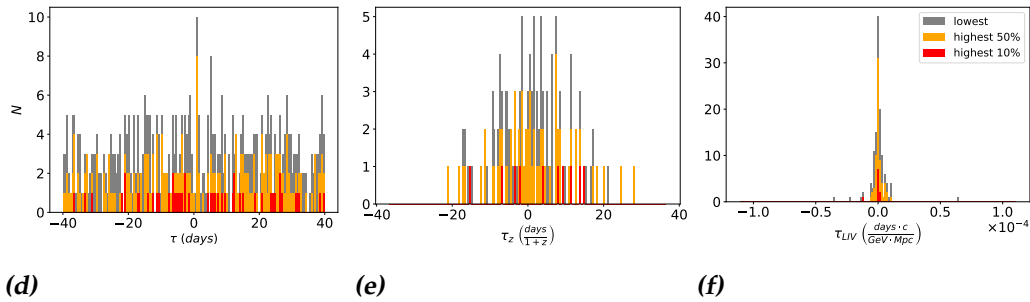


Figure 5.11: The stacked time differences for the three different physics cases. In plot a and d we see the time differences, τ , as measured. In plot b and e we see the probe of the time differences at the moment of emission τ_z . In plot c and f we see the Lorentz invariance probed time difference, τ_{LIV} in units of $\frac{\text{days}\cdot c}{\text{GeV}\cdot \text{Mpc}}$. The colors denote the energy selections used on selecting neutrino data.

Direction	f	P	P_z	P_{LIV}	N_{pairs}	$N_{z,pairs}$
<i>Up – going</i>	0%	0.34	0.70	0.40	44.3	11.6
	1%	0.40	0.73	0.42	45.3	11.9
	3%	0.70	0.80	0.52	48.3	12.7
	10%	1.0	0.95	0.80	58.4	15.6
	30%	1.0	1.0	1.0	86.8	23.7
<i>Down – going</i>	0%	0.80	0.73	0.75	27.4	5.3
	1%	0.86	0.77	0.79	28.4	5.5
	3%	0.98	0.86	0.87	31.4	6.5
	10%	1.0	0.98	0.98	39.3	8.9
	30%	1.0	1.0	1.0	63.3	16.2

Table 5.5: The probabilities P , P_z , and P_{LIV} to find values of $\psi > \psi_{data}$ for different injected fractions. The average number of matches per pseudo experiment is given by N_{pairs} , and for pairs with redshift $N_{z,pairs}$.

reject a signal associated to 3% of the GRBs with a confidence level of 52%. For the observed time difference of the down-going neutrinos we find that we can reject a signal associated to 3% of the GRBs with a confidence level of 98%. A signal in observed time difference over $1 + z$ associated to more than 3% of the GRBs can be rejected with a confidence level of 86%. For the LIV probed time difference, we can reject a signal associated to more than 3% of the GRBs with a confidence level of 87%. A signal associated to more than 30% of the GRBs can be rejected with a confidence level of 100% in both the northern and southern hemisphere, for all three scenarios probed. An overview of the confidence levels for the highest 10% energy neutrinos is given in table 5.5.

Even though we have now shown that any GRB to neutrino association is cannot be distinguished from a background result with any significance, we do the exercise of calculating the LIV scale and intrinsic time shift at the source. We follow the same approach of least squares fitting as for the IceCube 40 data in section 4.4.3. We have split up the results of this fit in those for up and down-going particles, and then considered the combined result in figures 5.12. The different parts of the sky are not in good agreement with each other. This again suggests that the association of GRBs to neutrinos was not significant over the background. Table 5.6 gives an overview of the found LIV scales and intrinsic time shifts. We have also shown the correlation coefficient, r_0 , which gives a measure of how well our data follows a linear distribution. In appendix B.1 we explain how

Fitting to find LIV scale

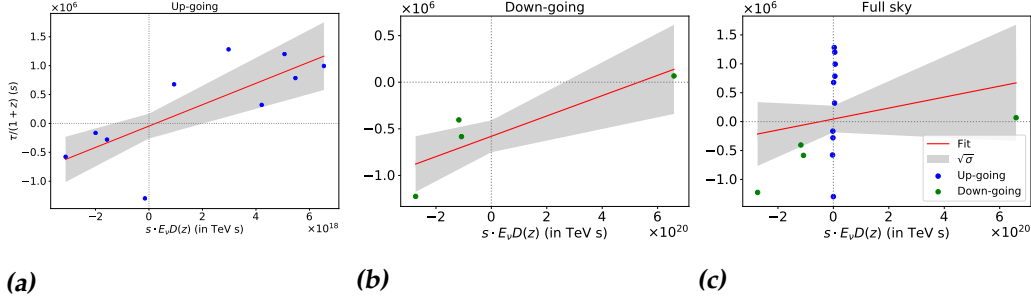


Figure 5.12: The least squares fitting approximation on the highest 10% energy neutrinos going both down and up in the detector. The slope of this fit corresponds to E_{LIV} and the zero crossing point corresponds to the intrinsic time shift.

Direction	E_{LIV} (GeV)	Δt_{in} (s)	r_0	$P(r > r_0)$
Up-going	$5.40 \pm 17.6 \cdot 10^{12}$	$-4.57 \pm 17.6 \cdot 10^4$	0.75	1.2%
Down-going	$9.17 \pm 21.4 \cdot 10^{14}$	$-5.80 \pm 1.71 \cdot 10^5$	0.86	14%
Full sky	$1.05 \pm 0.85 \cdot 10^{15}$	$4.49 \pm 23.0 \cdot 10^4$	0.23	44%

Table 5.6: The found LIV scale under the assumption that all neutrino to GRB associations are real LIV shifted GRB neutrinos.

we derived this coefficient. The probability to find a correlation coefficient bigger than the one found from our data in another uncorrelated data set with the same number of measurements is given by $p(|r| > |r_0|)$. We can see that both the up- and down-going neutrinos compare reasonably well with a linear relation. If we want to consider the sky as a whole however we find big discrepancies. The difference in neutrino energies is huge and hence both parts of the hemisphere will lead to a different result.

Conclusion

We have searched for a neutrino signal associated with a GRB using data from the IceCube detector and GRBweb. For this no model was assumed. Instead, we have allowed for an arrival time difference between the neutrino and its associated GRB photon counterpart of at most 40 days. To increase our chances of finding a signal over background we have used the cumulative timing profiles of all the neutrino to GRB associations we have found. We quantify how the found associations compare to a uniform background by using the timing profiles to calculate a test statistic.

We generate a large number of pseudo experiments by randomizing the actual neutrino data to find a lot of possible neutrino realizations. From these realizations, we can calculate the distribution function of the test statistic under different assumptions. We have shown that setting selection criteria on the neutrino energy can also increase our ability to distinguish a signal from background. For a signal consisting of 10% of GRBs that have a matching neutrino, we can increase our discovery power at the 3σ level by selecting only the highest 10% energy neutrinos. For up-going neutrinos our discovery power is increased from 3.1% to 87% and for down-going neutrinos it is increased from 4.3% to 78%.

We have not only investigated the association of neutrinos to GRB sources but also the possibility of changes in arrival times between a GRB photon and neutrino due to LIV. For this we considered a linear correction to the neutrinos velocity dispersion relation that scales with the neutrino energy divided by the LIV scale. We have probed the effects this factor can have on the observed arrival time differences between a photon and neutrino. To attain these results, we considered the arrival time difference, the arrival time difference corrected for redshift, and the arrival time difference corrected for the distance to the source and the neutrinos en-

ergy. A LIV effect is expected to be detected easiest in the last of these three scenarios. Applying the test statistic and an energy selection of only the highest 10% energy neutrinos we again improve our ability to distinguish signal from background. For probing LIV induced time shifts in a simulated signal associated to 30% we improve our discovery power for Up-going neutrinos from 0.035% to 26% at the 3σ level.

In the southern (northern) hemisphere we have found 352 (462) neutrino to GRB associations, including 103 (125) with a redshift measurement. Comparing this with our expectations from background, where we expect 304 (491) matches, including 123 (85) that have a redshift measurement, in the southern (northern) hemisphere. This signal is slightly lower than the expectations from our simulated background. Using the approach described in this thesis we are able to use this signal to reject the hypothesis that there is a neutrino signal associated to more than 30% of the GRBs, with a confidence level of 100%, in all three scenarios we probed.

If we only consider the high energy neutrinos we will find 23 matches with 4 redshift measurements in the northern hemisphere, and 48 matches with 10 redshift measurements. The p-values derived from the highest 10% energy neutrinos are given in table 5.5. The value found in our data always lies below the 3σ value from background which we have chosen to be the threshold of finding evidence for GRB neutrinos. We can therefore, not claim to have found a neutrino signal from GRBs in our data. We can however reject a signal consisting of matches to more than 30% of the GRBs. In the case of deriving a test statistic to probe time differences we can also neglect a signal to 10% of the GRBs. For the LIV case however our confidence in rejecting this signal is lower. For down-going neutrinos we have a P-value of 0.98 and for the up-going neutrinos only 0.80. A summary of the probabilities that a certain scenario matches the background is given in table 6.1

We have calculated the size of the LIV effect and an intrinsic time shift from associating the highest 10% energy neutrinos to GRBs. For this we assumed that all matches we have found are from GRB neutrinos. The matches observed in the northern and southern hemisphere allow for a linear fit with high correlation coefficient. Combining the two parts of the data however, leads to problems. From only up-going neutrinos we found a LIV scale of $E_{LIV} = (5.40 \pm 17.6) 10^{13} GeV$, and an intrinsic timeshift of $\Delta t_{in} = (-4.57 \pm 21.4) 10^4 s$ with $P(|r| > |r_0|) = 1.2\%$. For down-going neutrinos only we have found $E_{LIV} = (9.17 \pm 21.4) 10^{14} GeV$, and an intrinsic time shift of $\Delta t_{in} = (-5.8 \pm 1.71) 10^5 s$, with $P(|r| > |r_0|) = 14\%$.

Direction	E_f	P	P_z	P_{LIV}	N_{data}	$N_{data,z}$	N_{exp}	$N_{exp,z}$
Up– going	10%	0.34	0.70	0.39	48	10	44	12
	50%	0.57	0.29	0.58	232	69	233	60
	100%	0.85	0.60	0.56	462	125	490	123
Down– going	10%	0.80	0.73	0.75	23	4	27	5
	50%	0.09	0.12	0.18	171	45	149	33
	100%	0.12	0.42	0.04	352	103	304	85

Table 6.1: The probabilities P , P_z , and P_{LIV} to find values of $\psi > \psi_{data}$ for the different energy selection criteria. The average number of matches in the data is given by $N_{data(z)}$, and the number of matches expected from a background distribution is given by $N_{exp(z)}$.

Both parts of the sky separately strongly suggest a linear correlation between the data points. Part of this correlation is due to our own choice of changing the sign of the LIV term depending on the sign of the time difference. Considering the full hemisphere however, we find a LIV scale of $E_{LIV} = (2.24 \pm 1.44) 10^{15} GeV$, and an intrinsic time shift of $\Delta t_{in} = (-3.01 \pm 13.6) 10^4 s$ with $P(|r| > |r_0|) = 54\%$. We have confirmed our expectation, that we cannot derive a coherent value of the LIV scale using the data collected by IC79/86. We have done a similar analysis of the IC79/86 data in appendix C, but then with a constant search cone. This leads to even less power in distinguishing a signal over background in our data and further confirms our expectations.

6.1 Discussion

From analyzing IceCube data collected from June 2010 to May 2013 we cannot significantly separate a signal from background. On the contrary, we found slightly less matches than expected from a simulated background. We have however shown that using the method described in this work we can discern a signal coming from 10 to 30% of the GRBs. Since no assumption was made on neutrino emission in GRBs in this work, our method works best in distinguishing signal in the observed time difference. It is worth to consider how to improve the presented method to probe emission time differences. One way of going about this would be simulating signal with a given time difference and redshift at emission. This will make our test statistic less sensitive to the observed time differences but more sensitive to the observed time differences corrected for the redshift, and the LIV induced time differences.

If Lorentz invariance violation is the object of study, another possible improvement is promising to investigate. In this work, we have allowed for a maximum time window of ± 40 days. This was shown to be an estimated maximum value for LIV induced time shifts as observed on Earth, for IceCube data. The time shift was calculated from the LIV corrected velocity dispersion relation using values in the IC data that maximize it. Since this corrected velocity dispersion relation depends on the neutrinos energy it is interesting to consider the allowed time shift between a GRB photon and neutrino as a function of the neutrino energy. This will remove some of the matches found in this work that have a large observed time difference, but low energy.

The further completion of KM3NET might also give us insight in the association of neutrinos to cosmic sources. This detector will be able to distinguish a neutrino signal with a better angular resolution. This means that we can reduce the background for many of the GRBs in our data. The improved sensitivity might make even a single neutrino to GRB association significant. In [79] it is shown that km3net will be able to observe two gamma ray sources Vela jr. and RX J1713.7-3946 at 3σ significance within 6 and 5.5 years respectively.

Deriving the test statistic

This derivation follows the Bayesian assessment of the significance of a hypothesis given in [71, 73]. We will be using the test statistic, that is introduced by van Eijndhoven, as a reference to quantify our degree of believe in a hypothesis.

When considering two propositions A and B and some prior information I , we can write the probability that A is true under the condition that both B , and I are true, as $p(A|B, I)$. Using the product rule, $p(A, B|I) = p(A|I) p(B|A, I) = p(B|I) p(A|B, I)$, we can write this as Bayes' theorem [73].

$$p(A|B, I) = p(A|I) \frac{p(B|A, I)}{p(B|I)} \quad (\text{A.1})$$

Keeping this in mind we consider a hypothesis H , some observable data D and prior information I . We can use equation A.1 to find the posterior probability of hypothesis H , given by $p(H|D, I)$.

$$p(H|D, I) = p(H|I) \frac{p(D|H, I)}{p(D|I)} \quad (\text{A.2})$$

This is a function of the prior probability of hypothesis H given by $p(H|I)$, the likelihood function $p(D|H, I)$, and a normalization factor $p(D|I)$. The prior probability gives us a way of encoding the knowledge we have of a system. We can write down a similar expression for an alternative hypothesis, given by H_* , stating that H is not true. the ratio of the two probabilities is then given by

$$\frac{p(H|DI)}{p(H_*|DI)} = \frac{p(H|I) p(D|HI)}{p(H_*|I) p(D|H_*I)} \quad (\text{A.3})$$

We follow the suggestion in [71] of using a decibel scale to write an equation for the evidence of H relative to any alternative based on D and I .

$$e(H|D, I) = 10 \log \left[\frac{p(H|D, I)}{p(H_*|D, I)} \right] \quad (\text{A.4})$$

Using this with equation A.3 we can write

$$e(H|DI) = e(H|I) + 10 \log \left[\frac{p(D|H, I)}{p(D|H_*, I)} \right] \quad (\text{A.5})$$

The degree of believe to which our data supports a certain hypothesis is then given by the last term in equation A.5. We can now introduce the observables, $\psi = -10 \log p(D|H, I)$, which we will call the test statistic, and $\psi_* = -10 \log p(D|H_*, I)$. Since a probability always lies between 0 and 1 we have $\psi \geq 0$, and $\psi_* \geq 0$. We can finally write the evidence for H_* relative to H as

$$e(H_*|D, I) = e(H_*|I) + \psi - \psi_* \leq e(H_*|I) + \psi \quad (\text{A.6})$$

Here the value of ψ gives us a way of quantifying the degree of believe in hypothesis H . It is this test statistic that we will be using throughout this work to compare data against a number of hypotheses.

Appendix **B**

Least-squares fitting

If we want to find a relation between two measured observable quantities x and y of the form given in equation B.1. We start by noting that we have a limited amount of measurements N , and that we can denote every coordinate pair (x_i, y_i) . For every coordinate pair, we can write down a realization of equation B.1. If we know both A and B we can fill in a measured value of x_i and find the theoretical value y . The measured value of y_i is not exactly the same as the theoretical prediction. Instead it is expected to follow a normal distribution, of width σ_y around the theoretical value. We write the probability of finding a value single value y_i , in equation B.2, and of the whole set of measured $y_{1,2,3,\dots,N}$ values in equation B.3.

$$y = A + Bx \quad (\text{B.1})$$

$$P(y_i) \propto \frac{1}{\sigma_y} e^{-(y_i - A - Bx_i)^2 / 2\sigma_y^2}, \quad (\text{B.2})$$

or a collection of value χ ,

$$\begin{aligned} P(y_1, y_2, \dots, y_N) &= P(y_1) P(y_2) \dots P(y_N), \\ &\propto \frac{1}{\sigma_y^N} e^{-\chi^2 / 2}, \end{aligned} \quad (\text{B.3})$$
$$\chi^2 = \sum_{i=1}^N \frac{(y_i - A - Bx_i)^2}{\sigma_y^2}$$

We maximize the probability of finding the the values y_i we have in our data from this formula. This is done by minimizing χ^2 this with respect to both our unknown constants A and B . Solving the set of equations and

dropping the subscripts on the sum to make the formulas more readable gives equation B.4.

$$\begin{aligned} A &= \frac{\sum x^2 \sum y - \sum x \sum xy}{N \sum x^2 - (\sum x)^2}, \\ B &= \frac{N \sum xy - \sum x \sum y}{N \sum x^2 - (\sum x)^2} \end{aligned} \quad (\text{B.4})$$

Deriving the constants A and B we have used the assumption that y_i was normally distributed around some theoretical value with an width given by σ_y . This means that σ_y is given by the squared difference between the theoretical value and the measured value of y , divided by the number of degrees of freedom in our system. Equation B.5 shows σ_y . Note that this gives only information of the spread of points in our data, not on the actual errors of the data points, due to observational errors.

$$\sigma_y = \sqrt{\frac{1}{1-N} \sum (y - A - Bx)^2} \quad (\text{B.5})$$

Here A and B are given by equation B.4. We can now use this quantity to derive the uncertainties in the constants A and B by error propagation. We find

$$\begin{aligned} \sigma_A &= \sigma_y \sqrt{\frac{\sum x^2}{N \sum x^2 - (\sum x)^2}}, \\ \sigma_B &= \sigma_y \sqrt{\frac{N}{N \sum x^2 - (\sum x)^2}} \end{aligned} \quad (\text{B.6})$$

B.1 Correlation coefficient

The correlation coefficient gives us a measure of how well observed data can fit a linear relation. For a derivation of the equations used here see for example [77, 80]. It can be calculated considering how far individual data points, (x_i, y_i) lie from the median values (\bar{x}, \bar{y}) . It is calculated using the equation below.

$$r_0 = \frac{\sum (x_i - \bar{x})(y_i - \bar{y})}{\sqrt{\sum (x_i - \bar{x})^2 \sum (y_i - \bar{y})^2}} \quad (\text{B.7})$$

For points that are closely resembling a linear relation we expect to find $r_0 = \pm 1$, the zero denotes that this is from our data. If the data points

do not follow a linear relation we expect r_0 closer to zero. Now we still do not know how to interpret a value of r_0 if it is not equal to either ± 1 or 0. For any value in between the two extrema we have to compare our found result of r_0 , to that we find by considering the same number of uncorrelated points. We can then calculate what the probability is to find an uncorrelated r bigger than the one in our data with the equation below

$$P_N(|r| \geq |r_0|) = \frac{2}{\sqrt{\pi}} \frac{\Gamma((N-1)/2)}{\Gamma((N-2)/2)} \int_{|r_0|}^1 (1-r^2)^{(N-4)/2} dr \quad (\text{B.8})$$

Here N is the number of measurements in our data. r_0 is the observed value of the correlation coefficient, r is the correlation coefficient for uncorrelated data, and Γ is given by the integral below.

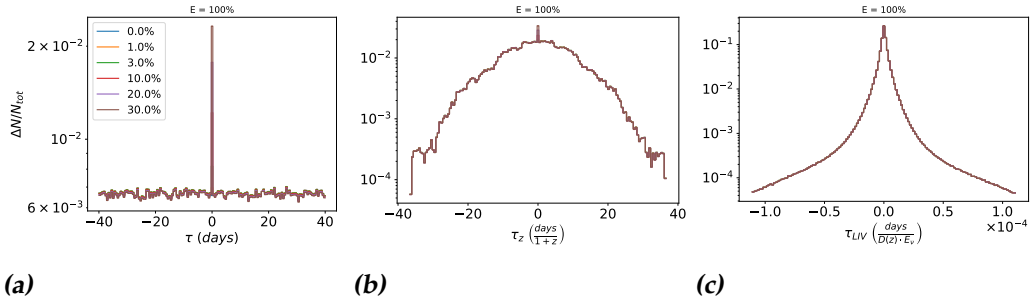
$$\int_0^\infty u^j e^{-au} du = \frac{\Gamma(j+1)}{a^{j+1}} \quad (\text{B.9})$$

Constant search cone on IC79/86

Here we show the results of associating IC79/86 neutrinos with GRBs using slightly different matching criteria. Instead of letting the search cone size vary depending on the positional error in our data, as was done in chapter 5, we have chosen to use a constant search cone size of 3° . In figure C.1 we have shown the timing profiles found by using 500.000 pseudo experiments. The test statistic derived from the pseudo experiments for the up-going events is given in figure C.2. The down-going events are shown in figure C.3.

The found matches for the unblinded data can be seen in figures C.4. The final values of the Lorentz violation scale are found by fitting a linear relation to the redshifted time difference as a function of the neutrino energies and the distance to the associated GRB source. This is shown in figure C.5 for both the up- and down-going events, and the combined data.

Stacked time differences of Up-going Neutrinos



Stacked time differences of Down-going Neutrinos

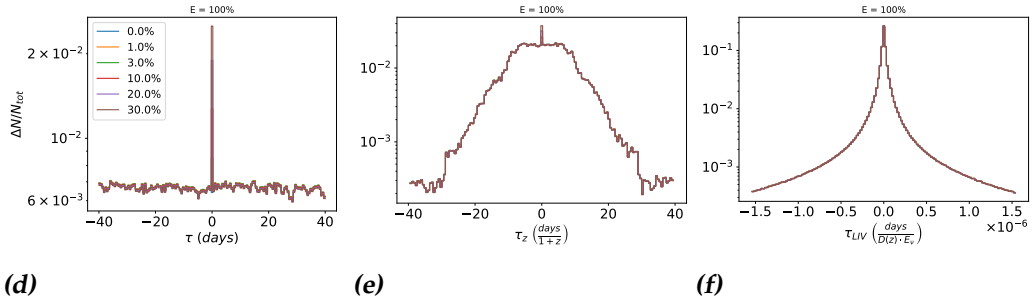


Figure C.1: The normalized stacked time differences of 500.000 realizations for the three different physics cases and different injected fractions of matching neutrinos in percentage. In plot a and d we see the time differences, τ , as observed. In plot b and e we see the time difference probe of the emission times τ_z . The redshift is used to extrapolate the observed time difference back to the emission time difference. In plot c and f we see the Lorentz invariance corrected time difference, τ_{LIV} in units of $\frac{\text{days} \cdot c}{\text{GeV} \cdot \text{Mpc}}$.

Distribution of the Test statistic for Up-going Neutrinos

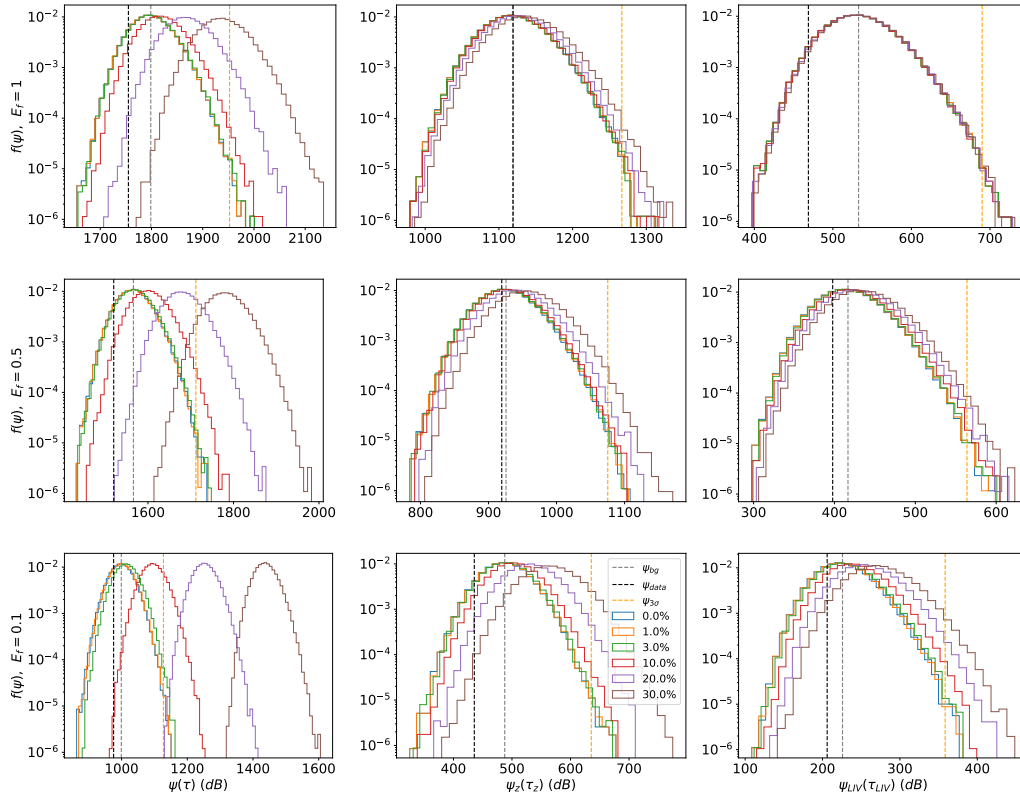


Figure C.2: From left to right we have shown the normalized distributions of ψ , ψ_z , and ψ_{LIV} for different fractions of simulated signal. The upper row gives the results if we include all neutrinos, the middle row gives the result if we include only the highest 50% energy neutrinos, and the bottom row gives the result for the highest 10% energy neutrinos. The dashed lines correspond to different threshold values. The mean from background, ψ_{bg} , is given in gray, the 3σ value is given in orange, and the black dashed line gives the value of, ψ_{data} we found in our data. An overview of the threshold values can be seen in tables C.1 and the probability of finding values above this threshold is given in table C.2. Note that the figures give up-going neutrinos only.

Threshold values of ψ for Up-going neutrinos

Selection		ψ_{bg}	ψ_{data}	$\psi_{3\sigma}$	$\langle N_{coinc} \rangle$	N_{data}
$E_f = 1$	τ	1799	1755	1952	2462	2325
	τ_z	1120	1119	1267	729	688
	τ_{LIV}	533	469	690	729	688
$E_f = 0.5$	τ	1566	1520	1712	1206	1177
	τ_z	926	919	1075	380	359
	τ_{LIV}	417	398	564	380	359
$E_f = 0.1$	τ	999	976	1127	236	240
	τ_z	488	436	635	79	63
	τ_{LIV}	226	206	358	79	63

Table C.1: The values of the test statistic as derived from the up-going neutrinos in the original data ψ_{data} , at the median from the background simulation, ψ_{bg} , and the 3σ limit from background. The expected number of coincidences, $\langle N_{coinc} \rangle$ in a background distribution and the found number of coincidences N_{data} are also given. Note that the results are given for the three different energy selections.

Probability of finding $\psi_{pseudo} > \psi_{bg}$ for Up-going Neutrinos

Selection	f	$1 - P_{bg}$	$1 - P_{3\sigma}$	$1 - P_{z,bg}$	$1 - P_{z,3\sigma}$	$1 - P_{LIV,bg}$	$1 - P_{LIV,3\sigma}$
$E_f = 100\%$	0%	0.49	0.00016	0.49	0.00016	0.48	0.00014
	1%	0.49	0.00016	0.49	0.00016	0.48	0.00013
	3%	0.51	0.00020	0.49	0.00018	0.48	0.00014
	10%	0.70	0.00090	0.52	0.00024	0.49	0.00014
	20%	0.97	0.027	0.58	0.00051	0.47	0.00015
	30%	1.0	0.37	0.68	0.0012	0.51	0.00018
$E_f = 50\%$	0%	0.49	0.00017	0.49	0.00015	0.48	0.00015
	1%	0.49	0.00016	0.49	0.00015	0.49	0.00016
	3%	0.53	0.00022	0.50	0.00015	0.50	0.00019
	10%	0.83	0.041	0.54	0.0031	0.55	0.00026
	20%	1.0	0.22	0.65	0.00091	0.63	0.00060
	30%	1.0	0.96	0.78	0.0036	0.70	0.0013
$E_f = 10\%$	0%	0.50	0.00017	0.50	0.00015	0.48	0.00015
	1%	0.52	0.00020	0.50	0.00016	0.49	0.00016
	3%	0.67	0.00082	0.53	0.00018	0.54	0.00022
	10%	1.0	0.18	0.67	0.00071	0.67	0.00092
	20%	1.0	1.0	0.87	0.0073	0.82	0.0040
	30%	1.0	1.0	0.97	0.062	0.91	0.014

Table C.2: This table gives the probability to find a value of the test statistic above the median from background, P_{bg} , for up-going neutrinos, and above the 3σ value from background, denoted by $P_{3\sigma}$. The probabilities are calculated for different injected fractions of signal, f , and for different energy selection criteria, E_f .

Distribution of the Test statistic for Down-going Neutrinos

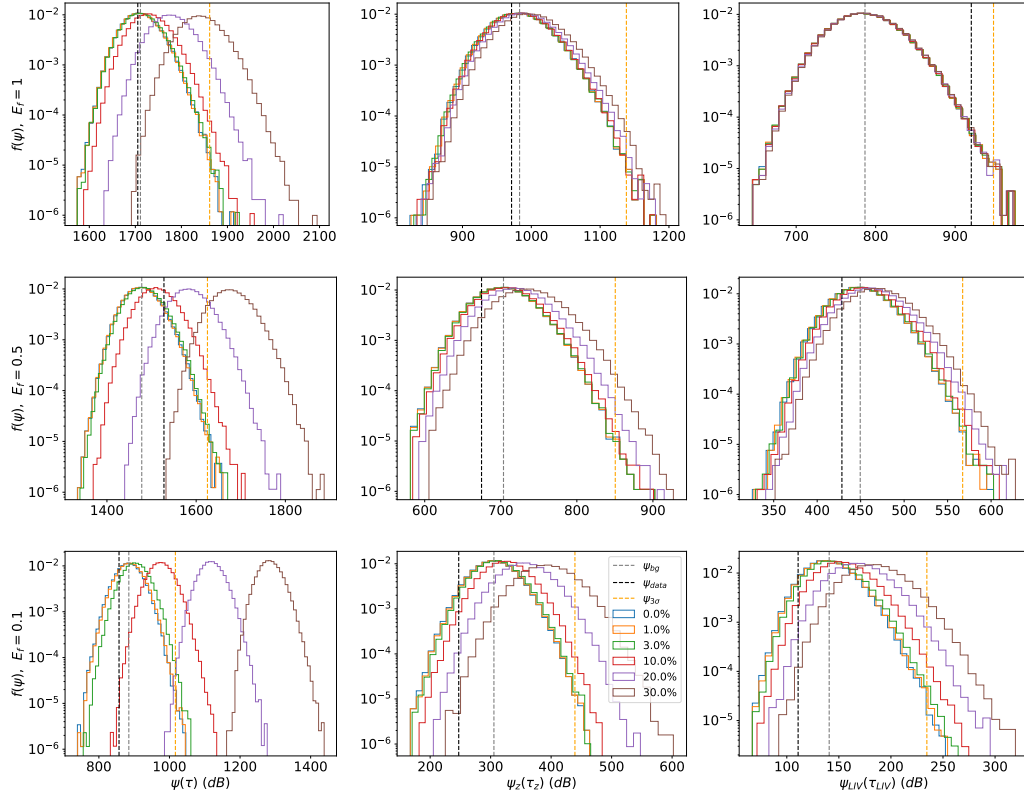


Figure C.3: From left to right we have shown the normalized distributions of ψ , ψ_z , and ψ_{LIV} for different fractions of simulated signal. The upper row gives the results if we include all neutrinos, the middle row gives the result if we include only the highest 50% energy neutrinos, and the bottom row gives the result for the highest 10% energy neutrinos. The dashed lines correspond to different threshold values. The mean from background, ψ_{bg} , is given in gray, the 3σ value is given in orange, and the black dashed line gives the value of, ψ_{data} we found in our data. An overview of the threshold values can be seen in tables C.3 and the probability of finding values above this threshold is given in table C.4. Note that the figures give down-going neutrinos only.

Threshold values of ψ for Down-going neutrinos

Selection		ψ_{bg}	ψ_{data}	$\psi_{3\sigma}$	$\langle N_{coinc} \rangle$	N_{data}
$E_f = 1$	τ	1711	1705	1861	1881	1960
	τ_z	983	971	1138	629	648
	τ_{LIV}	787	920	948	629	648
$E_f = 0.5$	τ	1478	1528	1625	924	928
	τ_z	704	675	851	248	242
	τ_{LIV}	450	428	567	248	242
$E_f = 0.1$	τ	885	857	1017	174	166
	τ_z	305	247	439	39	31
	τ_{LIV}	141	111	234	39	31

Table C.3: The values of the test statistic as derived from the down-going neutrinos in the original data ψ_{data} , at the median from the background simulation, ψ_{bg} , and the 3σ limit from background. The expected number of coincidences, $\langle N_{coinc} \rangle$ in a background distribution and the found number of coincidences N_{data} are also given. Note that the results are given for the three different energy selections.

Probability of finding $\psi_{pseudo} > \psi_{bg}$ for Down-going Neutrinos

Selection	f	$1 - P_{bg}$	$1 - P_{3\sigma}$	$1 - P_{z,bg}$	$1 - P_{z,3\sigma}$	$1 - P_{LIV,bg}$	$1 - P_{LIV,3\sigma}$
$E_f = 100\%$	0%	0.49	0.00015	0.49	0.00015	0.49	0.00016
	1%	0.49	0.00014	0.49	0.00015	0.49	0.00016
	3%	0.51	0.00023	0.49	0.00015	0.49	0.00015
	10%	0.69	0.0011	0.51	0.00016	0.49	0.00015
	20%	0.96	0.025	0.57	0.00023	0.50	0.00018
	20%	1.0	0.32	0.61	0.00070	0.50	0.00017
	$E_f = 50\%$	0%	0.49	0.00018	0.49	0.00015	0.49
1%		0.49	0.00019	0.49	0.00015	0.49	0.000156
3%		0.54	0.00027	0.50	0.00015	0.52	0.00022
10%		0.82	0.030	0.55	0.00019	0.58	0.00044
20%		1.0	0.16	0.67	0.00061	0.67	0.00098
20%		1.0	0.91	0.80	0.0029	0.75	0.0022
$E_f = 10\%$		0%	0.50	0.00016	0.49	0.00014	0.48
	1%	0.52	0.00019	0.50	0.00014	0.50	0.00023
	3%	0.70	0.00080	0.55	0.00019	0.56	0.00042
	10%	1.0	0.11	0.71	0.00095	0.72	0.0015
	20%	1.0	1.0	0.91	0.018	0.88	0.0095
	20%	1.0	0.91	0.99	0.15	0.96	0.042

Table C.4: This table gives the probability to find a value of the test statistic above the median from background, P_{bg} , for down-going neutrinos, and above the 3σ value from background, denoted by $P_{3\sigma}$. The probabilities are calculated for different injected fractions of signal, f , and for different energy selection criteria, E_f .

C.1 Results for constant search cone

In figure C.4 we show the found timing profiles from the IC79/86 data. The matching was done with a constant search cone. The p-values to find similar results from a background distribution are given in table C.5. From this we see that we find roughly the same number of matches in our data as we would expect from a background distribution. Depending on our energy selection criteria we find a difference in how well our data matches with the background expectations. From tables C.4 and C.2 we can see however, that the value of ψ_{data} will never be bigger than the 3σ threshold. Using the constant search cone we can again find the discovery power of distinguishing a signal associated to 10% of the GRBs. Similar to the varying search cone scenario described in chapter 5 we see that decreasing the total number of particles increases our ability to distinguish the background scenario from alternatives containing signal. If we compare the discovery power of the constant search cone to the varying search cone, we see that the discovery power to distinguish a signal associated to 10% of the bursts is much smaller. This is mainly due to the larger number of matches we find when we use a constant search cone. From this approach we see that our data cannot be distinguished from the background distribution. Using a constant search cone we make it even less likely to distinguish signal from background than using a varying search cone as described in chapter 4.2.1.

From the found matches in figures (c) and (f) in C.4, we can derive the LIV scale and intrinsic time shift. This is done in the same way as in section 5.4. The least squares fit is given in figure C.5 and the resulting values of the LIV scale and intrinsic time shift are given table C.6. As was explained in section 5.4 this is very different from the values found in [36].

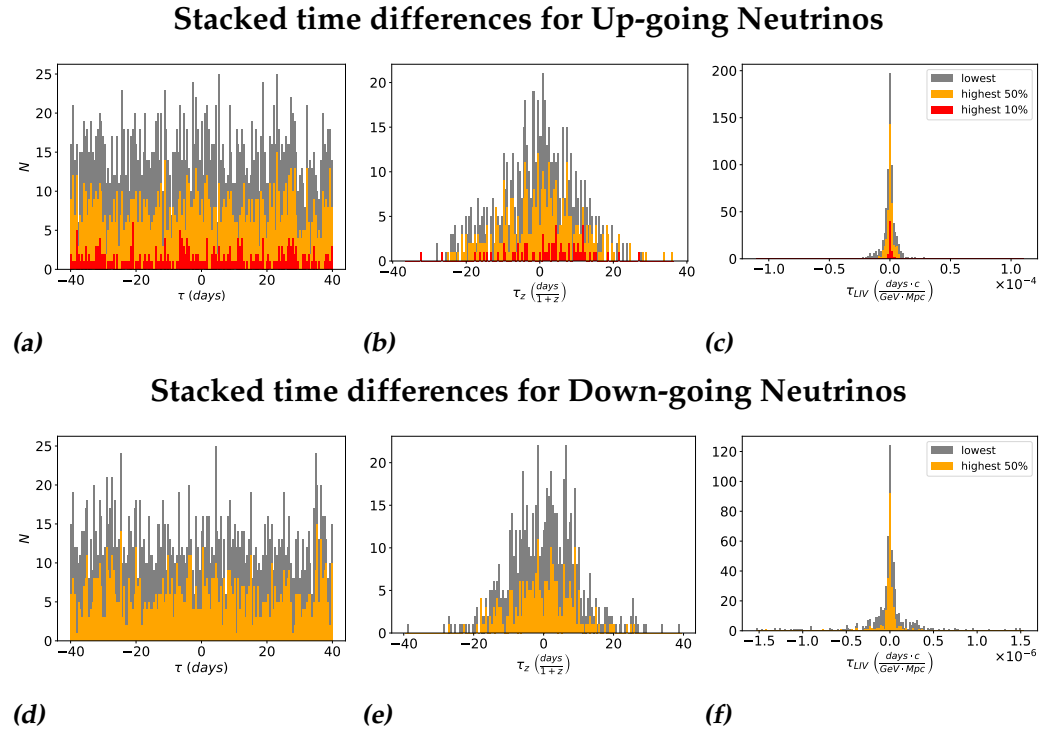


Figure C.4: The stacked time differences for the three different physics cases. In plot a and d we see the time differences, τ , as measured. In plot b and e we see the probe of the time differences at the moment of emission τ_z . In plot c and f we see the Lorentz invariance probed time difference, τ_{LIV} in units of $\frac{\text{days} \cdot c}{\text{GeV} \cdot \text{Mpc}}$. The colors denote the energy selections used on selecting neutrino data.

p-values found from comparing data with background.

Direction	E_f	P	P_z	P_{LIV}	N_{data}	$N_{data,z}$	N_{exp}	$N_{exp,z}$
Up–going	10%	0.75	0.92	0.48	240	63	236	79
	50%	0.90	0.56	0.70	1177	359	1206	380
	100%	0.88	0.49	0.96	2325	688	2462	729
Down–going	10%	0.79	0.96	0.92	166	31	174	39
	50%	0.09	0.79	0.76	928	242	924	248
	100%	0.55	0.61	0.0010	1960	648	1881	629

Table C.5: The probabilities P , P_z , and P_{LIV} to find values of $\psi > \psi_{data}$ for the different energy selection criteria. The average number of matches in the data is given by $N_{data(z)}$, and the number of matches expected from a background distribution is given by $N_{exp(z)}$.

Fitting to find LIV scale

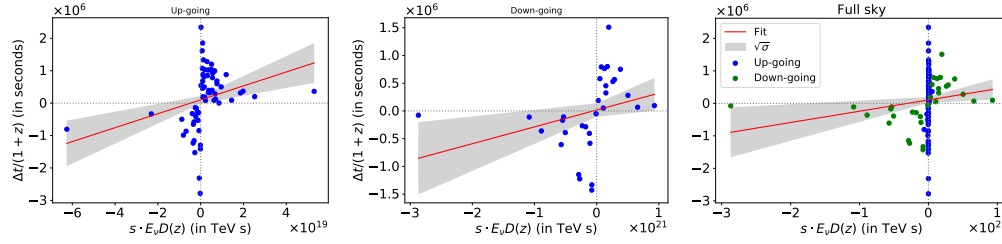


Figure C.5: The least squares fitting approximation on the highest 10% energy neutrinos going both down and up in the detector. The slope of this fit corresponds to E_{LIV} and the zero crossing point corresponds to the intrinsic time shift. The found values for each scenario are given in table C.6.

Direction	E_{LIV} (GeV)	Δt_{in} (s)	r_0	$P(r > r_0)$
Up-going	$0.47 \pm 1.07 \cdot 10^{14}$	$1.02 \pm 1.2 \cdot 10^5$	0.28	2.5%
Down-going	$3.29 \pm 5.42 \cdot 10^{15}$	$0.17 \pm 1.2 \cdot 10^5$	0.29	11%
Full sky	$2.88 \pm 4.23 \cdot 10^{15}$	$1.05 \pm 0.90 \cdot 10^5$	0.15	15%

Table C.6: The found LIV scale under the assumption that all neutrino to GRB associations are real LIV shifted GRB neutrinos.

Bibliography

- [1] T. Y. Cao, *References*, page 376â421, Cambridge University Press, 2 edition, 2019.
- [2] F. Abe et al., *Observation of Top Quark Production in $p p$ Collisions with the Collider Detector at Fermilab*, Phys. Rev. Lett. **74**, 2626 (1995).
- [3] S. Abachi et al., *Observation of the Top Quark*, Phys. Rev. Lett. **74**, 2632 (1995).
- [4] C. L. Cowan, F. Reines, F. B. Harrison, H. W. Kruse, and A. D. McGuire, *Detection of the Free Neutrino: a Confirmation*, Science **124**, 103 (1956).
- [5] G. Aad et al., *Observation of a new particle in the search for the Standard Model Higgs boson with the ATLAS detector at the LHC*, Phys. Lett. **B716**, 1 (2012).
- [6] G. R. Farrar and M. E. Shaposhnikov, *Baryon asymmetry of the Universe in the minimal standard model*, Phys. Rev. Lett. **70**, 2833 (1993).
- [7] S. Perlmutter, *Supernovae, Dark Energy, and the Accelerating Universe*, Physics Today **56**, 53 (2003).
- [8] S. Dodelson, *Modern cosmology*, Academic Press, San Diego, CA, 2003.
- [9] C. Rovelli, *Notes for a brief history of quantum gravity*, in *9th Marcel Grossmann Meeting on Recent Developments in Theoretical and Experimental General Relativity, Gravitation and Relativistic Field Theories (MG 9)*, pages 742–768, 2000.

-
- [10] G. Amelino-Camelia, C. Lämmerzahl, A. Macias, and H. Müller, *The Search for Quantum Gravity Signals*, in *Gravitation and Cosmology*, edited by A. Macias, C. Lämmerzahl, and D. Nunez, volume 758 of *American Institute of Physics Conference Series*, pages 30–80, 2005.
- [11] C. J. Isham, *Prima facie questions in quantum gravity*, volume 434, pages 1–21, Springer, Berlin, Heidelberg, 1994.
- [12] G. Amelino-Camelia and L. Smolin, *Prospects for constraining quantum gravity dispersion with near term observations*, *Phys. Rev. D* **80**, 084017 (2009).
- [13] G. Amelino-Camelia, D. Guetta, and T. Piran, *ICECUBE NEUTRINOS AND LORENTZ INVARIANCE VIOLATION*, *The Astrophysical Journal* **806**, 269 (2015).
- [14] J.-J. Wei, X.-F. Wu, H. Gao, and P. Mészáros, *Limits on the neutrino velocity, Lorentz invariance, and the weak equivalence principle with TeV neutrinos from gamma-ray bursts*, **2016**, 031 (2016).
- [15] G. Amelino-Camelia, J. Ellis, N. Mavromatos, D. Nanopoulos, and S. Sarkar, *Tests of quantum gravity from observations of gamma-ray bursts*, **393**, 763 (1998).
- [16] D. Mattingly, *Modern Tests of Lorentz Invariance*, *Living Reviews in Relativity* **8**, 5 (2005).
- [17] V. Vasileiou, A. Jacholkowska, F. Piron, J. Bolmont, C. Couturier, J. Granot, F. W. Stecker, J. Cohen-Tanugi, and F. Longo, *Constraints on Lorentz invariance violation from Fermi-Large Area Telescope observations of gamma-ray bursts*, *Phys. Rev. D* **87**, 122001 (2013).
- [18] J. Ellis, N. E. Mavromatos, D. V. Nanopoulos, and A. S. Sakharov, *Quantum-gravity analysis of gamma-ray bursts using wavelets*, **402**, 409 (2003).
- [19] U. Jacob and T. Piran, *Neutrinos from gamma-ray bursts as a tool to explore quantum-gravity-induced Lorentz violation*, *Nature Physics* (2007).
- [20] G. Amelino-Camelia and T. Piran, *Planck scale deformation of Lorentz symmetry as a solution to the UHECR and the TeV gamma paradoxes*, *Phys. Rev. D* **64**, 036005 (2001).
- [21] G. Amelino-Camelia and T. Piran, *Cosmic rays and TeV photons as probes of quantum properties of space-time*, *Phys. Lett. B* **497**, 265 (2001).

-
- [22] K. Hirata et al., *Observation of a neutrino burst from the supernova SN1987A*, Phys. Rev. Lett. **58**, 1490 (1987).
- [23] R. M. Bionta et al., *Observation of a neutrino burst in coincidence with supernova 1987A in the Large Magellanic Cloud*, Phys. Rev. Lett. **58**, 1494 (1987).
- [24] F. Capozzi, E. Lisi, A. Marrone, D. Montanino, and A. Palazzo, *Neutrino masses and mixings: Status of known and unknown $\hat{3}\hat{1}\hat{2}$ parameters*, Nuclear Physics B **908**, 218 (2016), Neutrino Oscillations: Celebrating the Nobel Prize in Physics 2015.
- [25] D. Eichler, M. Livio, T. Piran, and D. N. Schramm, *Nucleosynthesis, neutrino bursts and gamma-rays from coalescing neutron stars*, Nature (1989).
- [26] T. Piran, *Gamma-ray bursts a puzzle being resolved*, Physics Reports **333-334**, 529 (2000).
- [27] E. Waxman and J. Bahcall, *High Energy Neutrinos from Cosmological Gamma-Ray Burst Fireballs*, Phys. Rev. Lett. **78**, 2292 (1997).
- [28] J. Schmid, *Searches for High-Energy Neutrinos from Gamma-Ray Bursts with the ANTARES Neutrino Telescope*, PhD thesis, 2014.
- [29] S. Adrián-Martínez et al., *Stacked search for time shifted high energy neutrinos from gamma ray bursts with the ANTARES neutrino telescope*, Eur. Phys. J. **C77**, 20 (2017).
- [30] R. Abbasi et al., *A Search for a Diffuse Flux of Astrophysical Muon Neutrinos with the IceCube 40-String Detector*, Phys. Rev. **D84**, 082001 (2011).
- [31] P. Coppin, K. D. de Vries, and N. van Eijndhoven, *Identification of GRB precursors in Fermi-GBM bursts*, (2020).
- [32] b. nasa, <https://gcn.gsfc.nasa.gov/>.
- [33] J. Ellis, N. E. Mavromatos, A. S. Sakharov, and E. K. Sarkisyan-Grinbaum, *Limits on neutrino Lorentz violation from multimessenger observations of TXS 0506+056*, Physics Letters B **789**, 352 (2019).
- [34] Y. Huang, H. Li, and B.-Q. Ma, *Consistent Lorentz violation features from near-TeV IceCube neutrinos*, Phys. Rev. **D99**, 123018 (2019).

-
- [35] S. Mertens, *Direct Neutrino Mass Experiments*, Journal of Physics: Conference Series **718**, 022013 (2016).
- [36] Y. Huang and B.-Q. Ma, *Lorentz violation from gamma-ray burst neutrinos*, Communications Physics **1**, 62 (2018).
- [37] K. Olive, *Review of Particle Physics*, Chinese Physics C **40**, 100001 (2016).
- [38] S. Betts et al., *Development of a Relic Neutrino Detection Experiment at PTOLEMY: Princeton Tritium Observatory for Light, Early-Universe, Massive-Neutrino Yield*, arXiv e-prints , arXiv:1307.4738 (2013).
- [39] Z. Fodor, S. D. Katz, and A. Ringwald, *Relic neutrino masses and the highest energy cosmic rays*, Journal of High Energy Physics **2002**, 046 (2002).
- [40] B. Follin, L. Knox, M. Millea, and Z. Pan, *First Detection of the Acoustic Oscillation Phase Shift Expected from the Cosmic Neutrino Background*, **115**, 091301 (2015).
- [41] G. Steigman, *Neutrinos And Big Bang Nucleosynthesis*, arXiv e-prints , arXiv:1208.0032 (2012).
- [42] R. Davis, D. S. Harmer, and K. C. Hoffman, *Search for Neutrinos from the Sun*, Phys. Rev. Lett. **20**, 1205 (1968).
- [43] J. Ahrens et al., *Observation of high energy atmospheric neutrinos with the Antarctic muon and neutrino detector array*, Phys. Rev. D **66**, 012005 (2002).
- [44] T. K. Gaisser, *Atmospheric Neutrinos*, (2019).
- [45] E. Vitagliano, I. Tamborra, and G. Raffelt, *Grand Unified Neutrino Spectrum at Earth*, (2019).
- [46] J. S. Bloom, S. Kulkarni, and S. Djorgovski, *The Observed offset distribution of gamma-ray bursts from their host galaxies: A Robust clue to the nature of the progenitors*, Astron. J. **123**, 1111 (2002).
- [47] B. Paczynski and J. E. Rhoads, *Radio transients from gamma-ray bursters*, Astrophys. J. Lett. **418**, L5 (1993).
- [48] J. I. Katz, *Relativistic shock spectra: A Prediction*, Astrophys. J. Lett. **432**, L107 (1998).

- [49] M. Bottcher and C. D. Dermer, *High-energy gamma-rays from ultrahigh-energy cosmic ray protons in gamma-ray bursts*, *Astrophys. J. Lett.* **499**, L131 (1998).
- [50] P. Podsiadlowski, P. A. Mazzali, K. Nomoto, D. Lazzati, and E. Cappellaro, *The Rates of Hypernovae and Gamma-Ray Bursts: Implications for Their Progenitors*, *The Astrophysical Journal* **607**, L17 (2004).
- [51] R. W. Klebesadel, I. B. Strong, and R. A. Olson, *Observations of Gamma-Ray Bursts of Cosmic Origin*, *The Astrophysical Journal* **182**, L85 (1973).
- [52] T. Piran, *The Implications of the Compton (GRO) Observations for Cosmological Gamma-Ray Bursts*, *The Astrophysical Journal* **389**, L45 (1992).
- [53] J. Van Paradijs et al., *Transient optical emission from the error box of the γ -ray burst of 28 February 1997*, *Nature* **386**, 686 (1997).
- [54] D. Gruber et al., *THE FERMI GBM GAMMA-RAY BURST SPECTRAL CATALOG: FOUR YEARS OF DATA*, *The Astrophysical Journal Supplement Series* **211**, 12 (2014).
- [55] A. von Kienlin et al., *THE SECOND FERMI GBM GAMMA-RAY BURST CATALOG: THE FIRST FOUR YEARS*, *The Astrophysical Journal Supplement Series* **211**, 13 (2014).
- [56] P. N. Bhat et al., *THE THIRD FERMI GBM GAMMA-RAY BURST CATALOG: THE FIRST SIX YEARS*, *The Astrophysical Journal Supplement Series* **223**, 28 (2016).
- [57] S. Barthelmy et al., *The Burst Alert Telescope (BAT) on the Swift MIDEX mission*, *Space Sci. Rev.* **120**, 143 (2005).
- [58] S. D. Barthelmy, T. L. Cline, P. Butterworth, R. M. Kippen, M. S. Briggs, V. Connaughton, and G. N. Pendleton, *GRB Coordinates Network (GCN): A status report*, in *Gamma-ray Bursts, 5th Huntsville Symposium*, edited by R. M. Kippen, R. S. Mallozzi, and G. J. Fishman, volume 526 of *American Institute of Physics Conference Series*, pages 731–735, 2000.
- [59] A. Cucchiara et al., *A PHOTOMETRIC REDSHIFT OF $z \sim 9.4$ FOR GRB 090429B*, *The Astrophysical Journal* **736**, 7 (2011).
- [60] E. Waxman, *Cosmological Gamma-Ray Bursts and the Highest Energy Cosmic Rays*, *Phys. Rev. Lett.* **75**, 386 (1995).

-
- [61] P. D'Avanzo, *Short gamma-ray bursts: A review*, *Journal of High Energy Astrophysics* **7**, 73 (2015), *Swift 10 Years of Discovery, a novel approach to Time Domain Astronomy*.
- [62] J. X. Prochaska et al., *The Galaxy Hosts and Large-Scale Environments of Short-Hard Gamma-Ray Bursts*, *The Astrophysical Journal* **642**, 989 (2006).
- [63] M. G. Aartsen et al., *All-sky Search for Time-integrated Neutrino Emission from Astrophysical Sources with 7 yr of IceCube Data*, *The Astrophysical Journal* **835**, 151 (2017).
- [64] M. Aartsen et al., *Measurement of Atmospheric Tau Neutrino Appearance with IceCube DeepCore*, *Phys. Rev. D* **99**, 032007 (2019).
- [65] D. Chirkin and W. Rhode, *Propagating leptons through matter with Muon Monte Carlo (MMC)*, 2004.
- [66] M. G. Aartsen et al., *Energy reconstruction methods in the IceCube neutrino telescope*, *Journal of Instrumentation* **9**, P03009 (2014).
- [67] G. C. Hill, *First detection of high-energy astrophysical neutrinos with IceCube*, *AIP Conference Proceedings* **1666**, 040001 (2015).
- [68] M. Aartsen et al., *Measurement of the multi-TeV neutrino cross section with IceCube using Earth absorption*, *Nature* **551**, 596 (2017).
- [69] J. Formaggio and G. Zeller, *From eV to EeV: Neutrino Cross Sections Across Energy Scales*, *Reviews of Modern Physics* **84** (2013).
- [70] E. Rödel, Fisher, R. A.: *Statistical Methods for Research Workers*, 14. Aufl., Oliver & Boyd, Edinburgh, London 1970. XIII, 362 S., 12 Abb., 74 Tab., 40 s, *Biometrische Zeitschrift* **13**, 429 (1971).
- [71] N. Van Eijndhoven, *On the observability of high-energy neutrinos from gamma ray bursts*, *Astroparticle Physics* **28**, 540 (2008).
- [72] D. Bose, L. Brayeur, M. Casier, K. D. de Vries, G. Golup, and N. van Eijndhoven, *Bayesian approach for counting experiment statistics applied to a neutrino point source analysis*, *Astroparticle Physics* **50**, 57 (2013).
- [73] E. T. Jaynes, *Probability theory: the logic of science*.
- [74] J. Braun, M. Baker, J. Dumm, C. Finley, A. Karle, and T. Montaruli, *Time-dependent point source search methods in high energy neutrino astronomy*, *Astroparticle Physics* **33**, 175 (2010).

-
- [75] R. Abbasi, Y. Abdou, T. Abu-Zayyad, J. Adams, J. A. Aguilar Sánchez, M. Ahlers, K. Andeen, J. Auffenberg, X. Bai, M. Baker, S. Barwick, R. Bay, J. Alba, K. Beattie, J. Beatty, S. Bechet, J. Becker, K. Becker, M. L. Benabderrahmane, and S. Yoshida, *Search for Muon Neutrinos from Gamma-ray Bursts with the IceCube Neutrino Telescope*, *The Astrophysical Journal* **710**, 346 (2010).
- [76] J. D. Casey, *Search for high energy GRB neutrinos in IceCube*, PhD thesis, Georgia Institute of Technology, 2015.
- [77] J. Taylor and S. Taylor, *Introduction To Error Analysis: The Study of Uncertainties in Physical Measurements*, ASMSU/Spartans.4.Spartans Textbook, University Science Books, 1997.
- [78] P. H. Richter, *Estimating Errors in Least-Squares Fitting*, *Telecommunications and Data Acquisition Progress Report* **122**, 107 (1995).
- [79] S. Aiello et al., *Sensitivity of the KM3NeT/ARCA neutrino telescope to point-like neutrino sources*, *Astroparticle Physics* **111**, 100 (2019).
- [80] E. Pugh and G. Winslow, *The analysis of physical measurements*, by E.M. Pugh and G.H. Winslow, publisher not identified.